

LOCATION-BASED PROPAGATION MODELING FOR
OPPORTUNISTIC SPECTRUM ACCESS IN WIRELESS NETWORKS


by

Tugba Erpek
A Thesis
Submitted to the
Graduate Faculty
of
George Mason University
In Partial fulfillment of
The Requirements for the Degree
of
Master of Science
Electrical Engineering

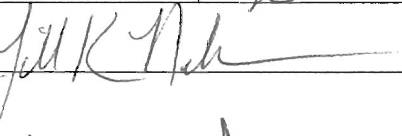
Committee:



Dr. Brian L. Mark, Thesis Director



Dr. Kathleen Wage, Committee Member



Dr. Jill Nelson, Committee Member



Dr. Andre Manitius, Chairman, Department
of Electrical Engineering



Dr. Lloyd J. Griffiths, Dean, The Volgenau
School of Information Technology and
Engineering

Date: 12/07/2007

Fall Semester 2007
George Mason University
Fairfax, VA

Location-based Propagation Modeling for Opportunistic Spectrum Access in Wireless
Networks

A thesis submitted in partial fulfillment of the requirements for the degree of Master of
Science at George Mason University

By

Tugba Erpek
Bachelor of Science
Osmangazi University, 2005

Director: Brian L. Mark, Associate Professor
Department of Electrical and Computer Engineering

Fall Semester 2007
George Mason University
Fairfax, VA

Copyright © 2007 by Tugba Erpek
All Rights Reserved

DEDICATION

To my parents, brother Can, sister Esra, and roommates Burcu and Astrid for all their support...

ACKNOWLEDGEMENTS

I would like to thank Dr. Mark for all his guidance during my graduate study. I always felt the privilege of having a supportive and encouraging professor throughout the two years I worked with him.

Thanks to my committee members, Dr. Wage and Dr. Nelson for always being kind to spare their valuable time to give feedback on my work.

Thanks to Ahmed Nasif for all his help and feedback on my thesis.

Thanks to Mark McHenry, Karl Steadman and Alexe Leu from Shared Spectrum Company for their helpful discussions and comments.

Thanks to my family for all their support during my study.

This work was supported by the U.S. National Science Foundation under Grant No. CCR-0209049 and Grant No. ECS-0426925.

TABLE OF CONTENTS

	Page
List of Tables.....	vi
List of Figures.....	vii
Abstract.....	viii
1. Introduction.....	1
2. Propagation Models	4
2.1 Empirical Propagation Model (EPM)-73	4
2.2 Okumura-Hata Model	5
2.3 Longley-Rice Model	6
2.4 Tirem Model	6
3. Location-Based Propagation Model	8
3.1 Tiling Algorithm	10
4. Application of LPM to Opportunistic Spectrum Access	28
4.1 Determining the Percentile of Loss for a Given Transmitter and Receiver.....	28
4.2 Using LPM to Determine MIFTP.....	34
5. Performance Evaluation of LPM	36
5.1 Memory Requirement	36
5.2 Violation Probability.....	37
5.3 Calculation Time.....	38
6. Spectrum Sensing via the Multitaper Method	41
6.1 Spectral Estimation	42
6.1.1 Conventional FFT Method.....	42
6.1.2 Multitaper Method	43
6.2 Numerical Results.....	45
7. Conclusion	54
Bibliography	57

LIST OF TABLES

Table	Page
Table 4.1.1 Grouping Distances into Distance Bins.....	30

LIST OF FIGURES

Figure	Page
Figure 3.1 Interference Caused to the Legacy User Receiver	9
Figure 3.1.1 Terrain Profile	11
Figure 3.1.2 Non-parametric pdf of Losses for the Whole Region	11
Figure 3.1.3 Whole Region Divided into Sub-areas.....	12
Figure 3.1.4 Non-parametric pdf of Losses for Sub-areas.....	13
Figure 3.1.5 Whole Region Divided into Quadrants	14
Figure 3.1.6 Non-parametric pdf of Losses for Quadrants	14
Figure 3.1.7 Initial Seed	17
Figure 3.1.8 First Percentile of Loss Distribution for the Initial Seed.....	17
Figure 3.1.9 Diagonal Increase of the Seed Size	18
Figure 3.1.10 Diagonal Binary Search – Mean Seed Length is Found.....	19
Figure 3.1.11 Diagonal Binary Search – Check the Difference Between L and L_o	20
Figure 3.1.12 Diagonal Binary Search – Continue if the Initial Criteria is not Satisfied	20
Figure 3.1.13 Diagonal Binary Search – Optimum Seed Size is Determined Diagonally.....	21
Figure 3.1.14 Horizontal Growth	22
Figure 3.1.15 Horizontal Binary Search	23
Figure 3.1.16 Vertical Growth.....	24
Figure 3.1.17 Vertical Binary Search	25
Figure 3.1.18 Tiled Region.....	26
Figure 3.1.19 Tiled Region with Overlapping Sub-areas	27
Figure 4.1.1 Numbered Tiles.....	28
Figure 4.1.2 Transmitter and Receiver Pair in the Same Tile.....	31
Figure 4.1.3 Transmitter and Receiver Pair in Different Tiles	33
Figure 5.3.1 A Given Transmitter and Receiver Far Away From Each Other	39
Figure 5.3.2 A Given Transmitter and Receiver Close to Each Other	39
Figure 6.2.1 Max-Hold Plot for TV Channel 3 Using the FFT Method.....	46
Figure 6.2.2 Max-Hold Plot for TV Channel 3 Using the MT Method.....	46
Figure 6.2.3 Number of correctly identified busy channels vs. Threshold Value	50
Figure 6.2.4 Number of False Alarm Channels vs. Threshold Value.....	51
Figure 6.2.5 Number of Miss-Detected Channels vs. Threshold Value	52
Figure 6.2.6 Number of Correctly Identified Free Channels vs. Threshold Value.....	53

ABSTRACT

LOCATION-BASED PROPAGATION MODELING FOR OPPORTUNISTIC SPECTRUM ACCESS IN WIRELESS NETWORKS

Tugba Erpek, M.S.

George Mason University, 2007

Thesis Director: Dr. Brian L. Mark

Wireless spectrum has become a scarce resource due to the exponential growth of the number and type of devices that utilize the electromagnetic spectrum. The cost of long term leasing of spectrum has proven to be a major road block in efficient use of frequency spectrum. Moreover, spectrum measurement studies have shown that substantial portions of the allocated wireless spectrum are highly underutilized. Thus, Dynamic Spectrum Access (DSA) devices have been proposed to be allowed to share the spectrum dynamically between users. The idea is that the DSA devices will continuously scan the spectrum and start to transmit in a channel when a licensed user's operation is not detected in that channel. Detailed path loss models are needed to calculate the propagation loss between a DSA device transmitter and a licensed user receiver in order for the DSA device to avoid causing interference to the receiver by using overly high transmit power levels.

This thesis proposes a novel propagation loss model called Location Based Propagation Modeling (LPM) based on the existing TIREM path loss model. The TIREM model gives the median value of the path loss for a given transmitter and receiver pair and the user needs to know the precise locations of the transmitter and receiver to calculate the path loss with the TIREM model. However, for DSA applications, we usually do not know the precise locations of the licensed user receivers. Furthermore, TIREM model requires detailed terrain information stored in the memory to calculate path loss, but DSA devices have limited memory. As a result, we need a compact representation of the TIREM model which gives the path loss without the need to store terrain information in the memory. These were the motivations to develop the LPM.

DSA devices require accurate spectral estimation methods to determine whether a channel is occupied in a specific time and location. Two spectral estimation methods: multitaper spectral estimation method and conventional FFT-based spectral estimation method are compared in this thesis using real signal measurements. Our numerical results show that the multitaper approach yields a significant increase in the number of harvested channels, while maintaining a smaller probability of false alarm.

Chapter 1: Introduction

The electromagnetic radio spectrum is a natural resource and the use of transmitters and receivers is licensed by governments [1]. Currently, wireless spectrum is partitioned into fixed frequency bands by the Federal Communications Commission (FCC). Over the last decade, it has become a highly valued resource due to the exponential growth of the wireless communications industry. Moreover, spectrum measurement studies have shown that substantial portions of the allocated wireless spectrum are highly underutilized [2]. As a result, the approach of partitioning the spectrum into fixed frequency bands causes a waste of wireless resources.

Dynamic Spectrum Access (DSA) is a promising approach to increase the efficiency of the spectrum usage. This approach allows unlicensed wireless users to access the licensed bands from the legacy spectrum holders on an opportunistic basis [3]. The idea is that the DSA devices will continuously scan the frequency spectrum and start to transmit in a channel when the licensed users do not transmit at that frequency. Furthermore, DSA devices will abandon the channel that they transmit within a certain time when they sense the legacy user's activity on the same channel again. DSA technology makes use of various capabilities such as frequency agility, adaptive modulation, and transmit power control. These features allow the DSA devices to

communicate efficiently while minimizing the interference level to the legacy user devices.

DSA radios need to determine the maximum possible power level that avoids the harmful interference at the legacy user receivers. This power level is called Maximum Interference Free Transmit Power (MIFTP) [2]. For a given transmit power, the path loss is calculated using the propagation loss models and the interference level at the legacy user receiver is estimated. Consequently, the accuracy of the path loss model used is very important when determining the maximum power level of DSA transmitters such that they will not interfere with the operation of licensed users.

There are two classes of propagation loss models: empirical models and deterministic models. Empirical models are based on measured and averaged losses along typical classes of radio links. Empirical Propagation Model (EPM-73) and Okumura – Hata model are examples of empirical path loss models. Deterministic methods are based on the physical laws of wave propagation and these methods produce more accurate and reliable predictions of path loss compared to statistical methods. However, detailed and accurate description of all objects in the propagation space is required for deterministic methods; as a result, they are more expensive in computational effort. For instance, Longley-Rice and TIREM path loss models are based on deterministic path loss models combined with empirical measurements.

A novel path loss model called Location Based Propagation Modeling (LPM) is presented in this thesis. The path loss models such as Longley-Rice and TIREM model in the literature give the median loss value for a given distance between a transmitter and

receiver pair. The user needs to know the precise locations of the transmitter and receiver to calculate the path loss with these models. However, the precise transmitter and/or receiver locations are usually not known in spectrum sharing applications. Moreover, TIREM and Longley-Rice models require detailed terrain information to calculate path losses, but DSA devices have limited memory. These were the motivations to develop LPM, which does not require precise locations of the transmitter and receiver. Moreover, LPM does not require a lot of memory space to store the detailed terrain data.

In LPM, a given area is first divided into smaller sub-areas (called tiles), which have similar terrain features. Then, the probability density functions of losses are obtained for each tile by sampling loss values. By using tiles, the local terrain characteristics are reflected more accurately than if a single pdf were used to represent the entire coverage area. Furthermore, the location uncertainty problem is solved with the tiling approach.

A survey of the well-known propagation models is provided and their advantages and disadvantages are discussed in Chapter 2. The LPM model and tiling algorithm are explained in Chapter 3. Application of LPM to opportunistic spectrum access is explained in Chapter 4 and a performance evaluation of LPM is given in Chapter 5. Spectrum sensing via the multitaper method is discussed in Chapter 6 and conclusions are given in Chapter 7.

Chapter 2: Propagation Models

The power intensity of an electromagnetic wave reduces when it propagates through space. This attenuation in power intensity is called *path loss*. Path loss may be due to many effects, such as free space loss, refraction, diffraction, reflection, aperture-medium coupling loss, and absorption [4]. A radio propagation model is a mathematical formulation for the characterization of path loss as a function of frequency, distance and other conditions. Different models have been developed to meet the needs of realizing the propagation behavior in different conditions.

2.1 Empirical Propagation Model (EPM-73)

Empirical Propagation Model (EPM-73) is an empirical propagation model that has the advantage of simplicity of manual calculations of basic transmission loss. In many cases, detailed terrain data is not available and in some cases path loss calculations are required for mobile devices. EPM-73 is a model that provides reasonably accurate estimates of expected losses with minimal input information. Only antenna heights, frequency and path-length information are required as the input parameters while calculating the loss. For the frequency range of 20–100 MHz, the path loss predictions from EPM-73 are as good as those produced using more complicated models [5].

2.2 Okumura - Hata Propagation Model

The Okumura – Hata model is the most widely used empirical propagation loss model in radio frequency propagation to predict the behavior of cellular transmission in urban areas that have a high building density. The input parameters for the model include frequency, antenna height of base station, antenna height of mobile station and the distance between the base station and the mobile station. The locations of the transmitter and receiver are not required to calculate the loss in this model. The terrain size (small, medium, large) and type (urban, suburban, open) are also specified by the user as input parameters while calculating loss [6].

There are some restrictions while specifying input parameters of the Okumura - Hata model. For instance, the input frequency must be between 150 MHz and 1000 MHz. Moreover, the distance between the transmitter and receiver must be between 1 km and 20 km. As a result, the model is accurate only when the distance between the transmitter and receiver is less than 20 km. The antenna height of the base station must be between 30 m and 200 m and the antenna height of the mobile station must be between 1 m and 10 m to obtain reasonable predictions.

As only four parameters are required for the Okumura-Hata model, the computation time is short. This is an advantage of this model. However, the model neglects the terrain profile between transmitter and receiver, i.e., hills or other obstacles between the transmitter and the receiver are not considered. Phenomena like reflection and shadowing are not included in the model, as well. Free space loss and diffraction by the smooth earth are extensively treated while calculating the loss with this model.

2.3 Longley-Rice Propagation Model

The Longley – Rice propagation loss model is a general purpose model based on electromagnetic theory and on statistical analyses of both terrain features and radio measurements. It has been adopted as a standard by the FCC to evaluate TV service coverage [7]. The model predicts the median transmission loss of a radio signal as a function of distance and the variability of the signal in time and in space over irregular terrain between 20 MHz and 10 GHz. The model uses free-space loss, diffraction by smooth earth, reflection from earth surface, and atmospheric refractivity to give the median value of losses.

The Longley – Rice path loss model has two parts: a model for predictions over an area and a model for point-to-point link predictions. The point-to-point prediction requires detailed terrain information. The set of parameters that must be defined to find a particular path loss include frequency, polarization, path length, antenna heights above ground, surface refractivity, effective earth's radius, climate, ground conductivity, and ground dielectric constant. Precise locations of transmitter and receiver are required for this model. If a detailed terrain path profile is not available, the resulting prediction is called 'area' mode prediction [8].

2.4 TIREM Propagation Model

Terrain Integrated Rough Earth Model (TIREM) predicts radio frequency propagation loss over irregular terrain and seawater for ground-based and air-borne transmitters and receivers [9]. The model is in the form of a computer program and a

digitized database of terrain elevations is required for the model. The inputs to the program are frequency (40 MHz to 20 GHz), polarization, ground permittivity and conductivity, atmospheric refractivity modulus, absolute humidity, and transmitter and receiver antenna structural heights, site elevations, latitudes and longitudes. The program gives the median path loss and fading statistics as outputs. The techniques used to calculate the median loss are free space spreading, reflection, diffraction, surface-wave, tropospheric-scatter, and atmospheric absorption. The model applies when either the transmitter or the receiver is below 30,000 meters. The precise transmitter and receiver locations are required by the model and the computation time is proportional to the terrain resolution.

The path loss values obtained using TIREM and Longley-Rice model are very close to each other. However, the TIREM model is usually the preferred path loss model for tactical military radios for the Department of Defense.

Chapter 3: Location-Based Propagation Model (LPM)

TIREM path loss model is a complex propagation model and takes the latitude, longitude and elevation data into account while calculating path loss values and gives the median path loss value as output. This model requires detailed terrain information stored in the memory in advance to calculate path loss. However, DSA devices have limited memory and storing the terrain data for a very large region is not possible. A ‘compact’ path loss model which provides the same accuracy as a deterministic model and occupies less memory is required.

Additionally, the user needs to know the precise locations of the transmitter and receiver to calculate the path loss with TIREM model, but there is location uncertainty in spectrum sharing applications. As a result, we have to take this uncertainty into account to calculate MIFTP. We represent the location uncertainty in terms of probability density function (pdf) of loss values for a given distance with LPM.

DSA radios are planned to be used in TV bands and the locations of TV transmitters are known in advance, but the precise locations of the receivers are not known. As a result, DSA devices have to be conservative while calculating MIFTP to minimize the interference level at legacy user receiver. Figure 3.1 illustrates a scenario where a DSA node transmitter causes interference to the legacy user receiver.

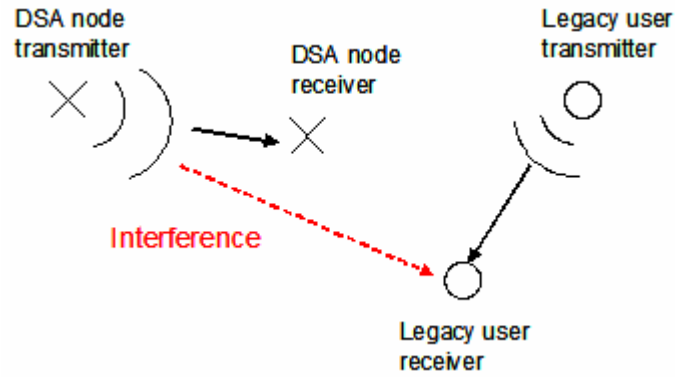


Figure 3.1 Interference Caused to the Legacy User Receiver.

The pdfs of loss values help DSA devices to determine MIFTP in case there is not enough information about the locations of legacy user receivers. Low percentiles of pdf of losses, i.e., 1st percentile, should be used to determine MIFTP if the terrain and location information is not sufficient. In other words, by using pdf of losses, the user knows how much conservative the DSA device needs to be in order not to affect the operation of legacy users.

The memory requirement and location uncertainty in spectrum sharing applications were the main motivations to obtain a new approach called Location-Based Propagation Model (LPM), based on the existing TIREM model. LPM model uses a tiling algorithm which is explained in detail in the next section.

3.1 Tiling Algorithm

LPM path loss model includes tiling algorithm. A given area is divided into sub-areas according to some user defined criteria and the loss data for each sub-area is stored in the memory for the tiling algorithm.

The path loss values are heavily dependent on the area where the transmitters and receivers are located. Thus, the path loss can be very different between two transmitter and receiver pairs in an urban and open area even though they have the same distance between each other. Figure 3.1.1 is obtained using the real terrain data. The measurements for the terrain data were taken in Virginia and Maryland in U.S. between the latitudes of 38° and 40° , and the longitudes of -80° and -76° . For instance, if we choose 2,000 uniformly distributed transmitter and receiver pairs with a fixed distance of 20 km between each other in the area shown in Figure 3.1.1 and calculate the path loss values using TIREM path loss model, we obtain the non-parametric probability density function of losses given in Figure 3.1.2. Normalized histograms are used to obtain the non-parametric pdfs.

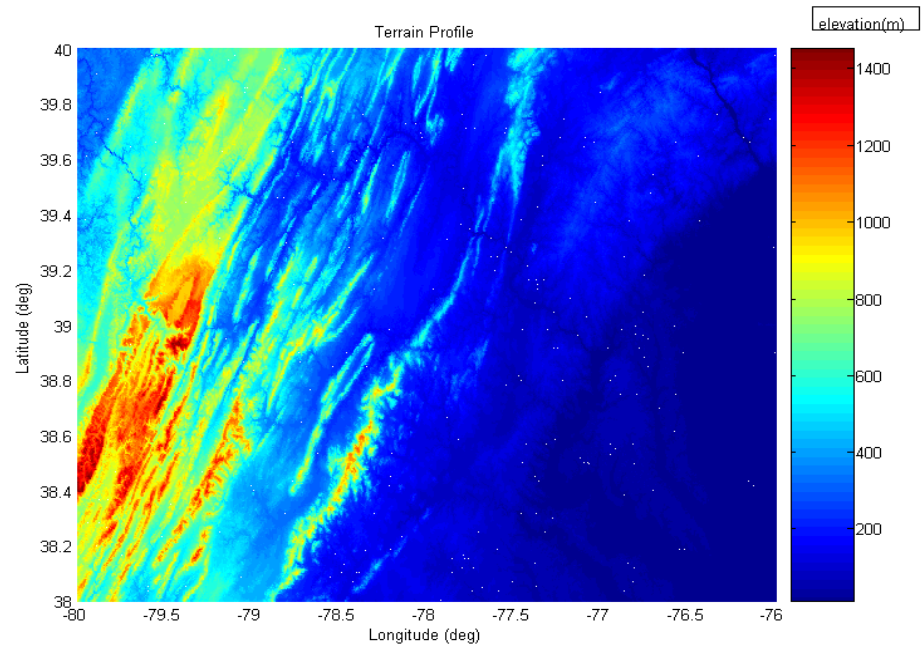


Figure 3.1.1 Terrain Profile.

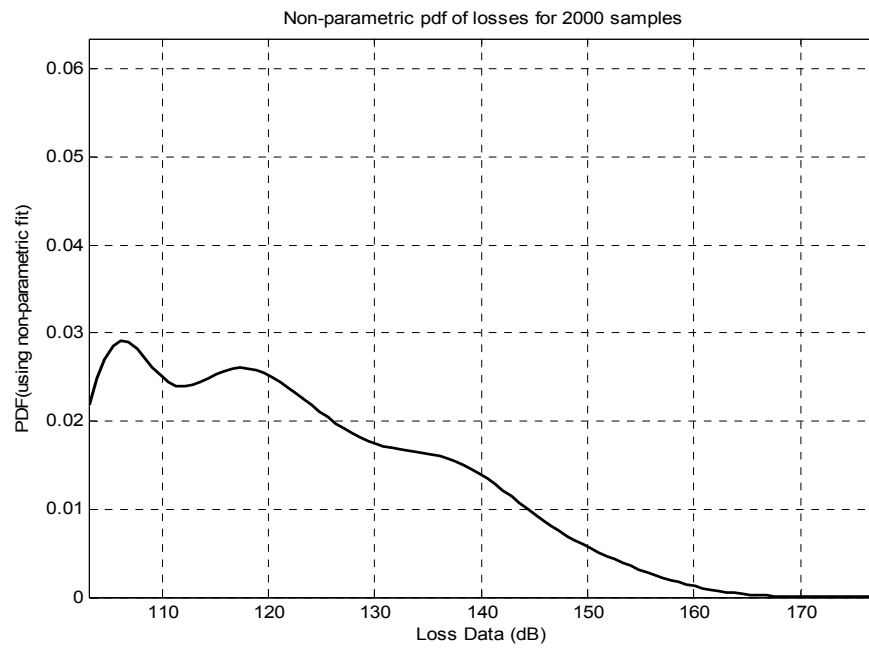


Figure 3.1.2 Non-parametric pdf of Losses for the Whole Region.

Furthermore, if the region of interest is divided into smaller areas as in Figure 3.1.3, it can be seen that the non-parametric pdf of losses for the small areas are quite different compared to the one for the whole region. The plots of non-parametric pdfs of losses are given in Figure 3.1.4.

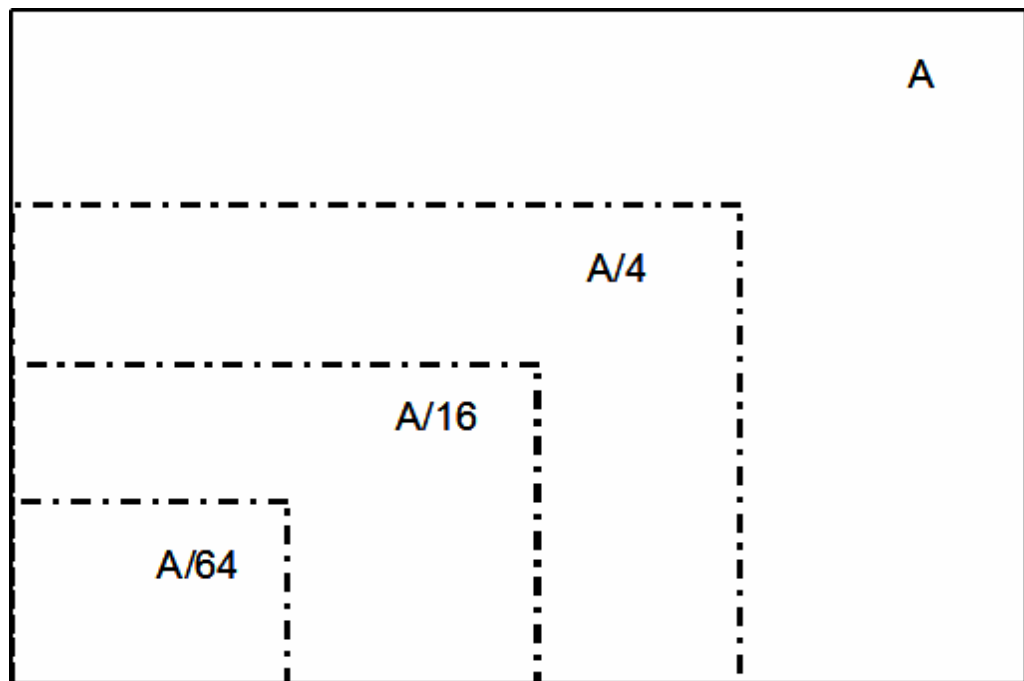


Figure 3.1.3 Coverage Area Divided into Sub-areas.

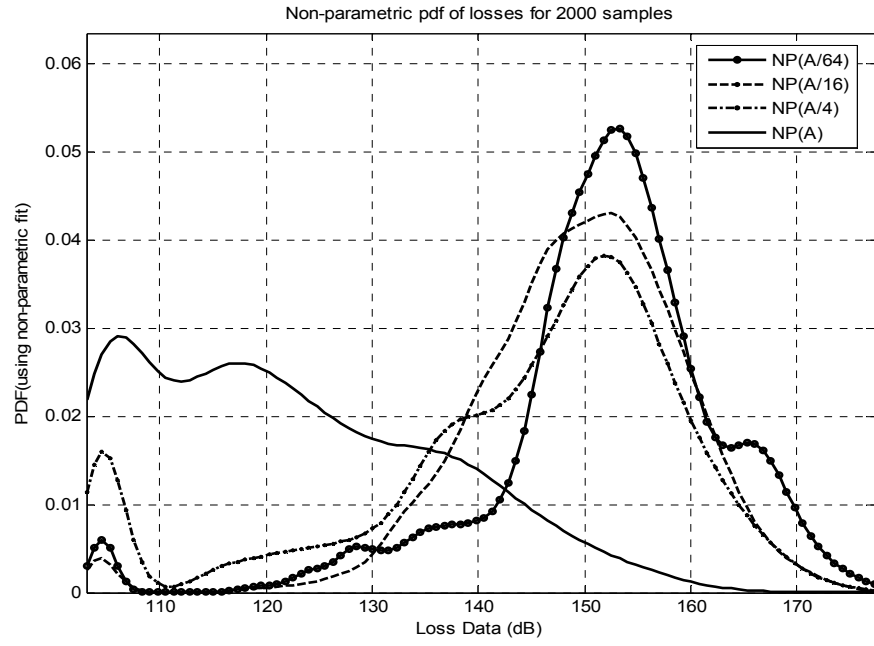


Figure 3.1.4 Non-parametric pdf of Losses for Sub-areas.

As another example, when we divide the given region into quadrants as shown in Figure 3.1.5, the non-parametric pdfs of losses are given in Figure 3.1.6. The pdf of losses change significantly when the size of the area of interest is increased.

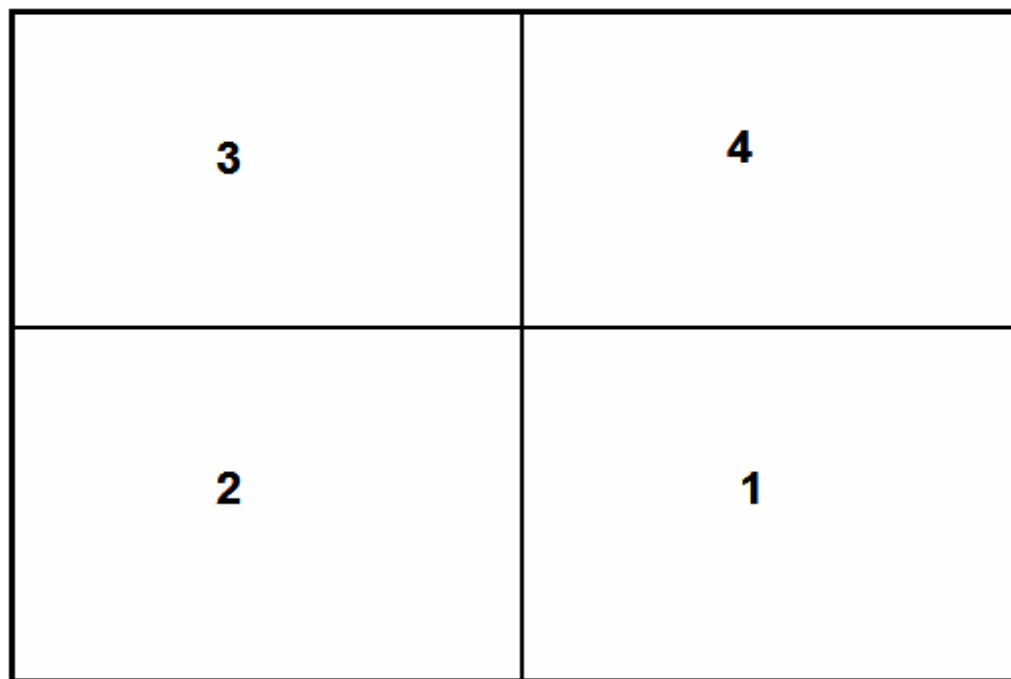


Figure 3.1.5 Whole Region Divided into Quadrants.

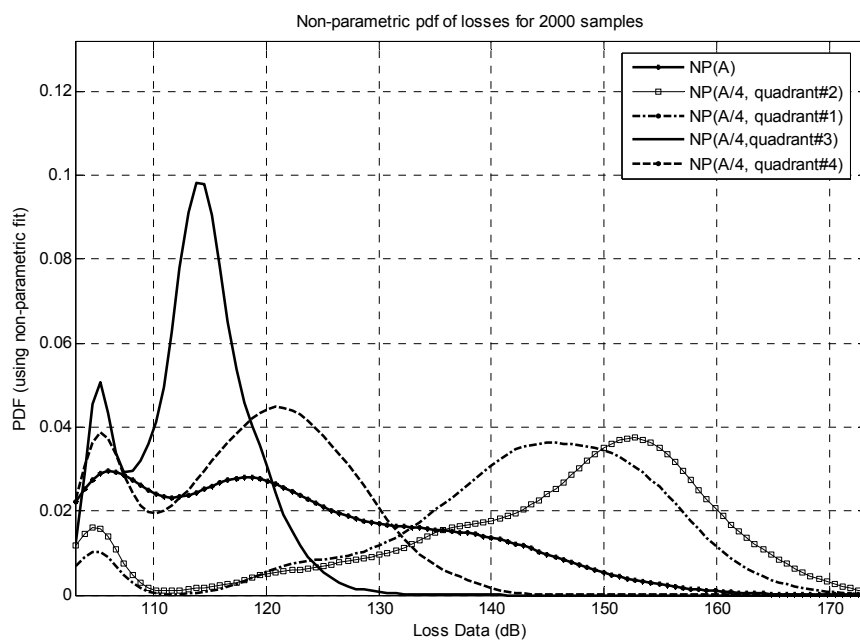


Figure 3.1.6 Non-parametric pdf of Losses for Quadrants.

Consequently, since pdf of losses are calculated for the areas that have similar terrain characteristics in the tiling approach, the resulting pdfs of losses reflect the terrain features better.

The tiling algorithm divides a given area into sub-areas according to user defined criteria and stores the mean and variance values of the probability loss distributions in the memory for each distance bin in each tile. All the path loss calculations are done in advance and the mean and the variance values for the loss distributions, which are output parameters of tiling algorithm, are stored in the memory.

Suppose we approximately know the location of the DSA node transmitter, but we don't know the location of the legacy user receiver. Furthermore, we need to calculate the path loss between the transmitter and receiver in order to determine the MIFTP. Since we have some information about the location of the transmitter, we choose the tile that covers this transmitter location and retrieve the path loss value from the memory for the corresponding distance bin. In addition, the user can choose different percentiles of the pdf of losses while obtaining the path loss. The chosen percentile value depends on the application and the amount of information the user has for the approximate location of the legacy user receiver. The probability of harmful interference to the legacy user receiver decreases with this approach.

The user specifies the latitude, longitude and elevation data for the region of interest, the minimum and maximum distance between the transmitter and receiver pairs, the frequency range, the transmitter and receiver antenna heights and the polarization of the antennas at the beginning of the program.

In tiling algorithm, first, initial seed size is specified (Figure 3.1.7). The initial seed is a square with a seed length of $\sqrt{2} * d_{\max}$ where d_{\max} is equal to the maximum distance value that the user specifies as one of the input parameters. Once the initial seed size is determined, a user-specified number of transmitter and receiver pairs are chosen in the seed and the path losses are calculated for each of these pairs using TIREM path loss model. If the user chooses a small number of transmitter and receiver pairs in the area, then a different tiling will be obtained in each execution of the code since the chosen samples will reflect different features of the terrain. On the other hand, if a very large number of samples are chosen, then the time to compute the LPM model will be more. The user should decide to the number of samples in the area depending on the application.

After calculating the path losses between transmitters and receivers, the probability density functions of the loss values are approximated using normal pdfs, because the normal pdfs fit the distribution of losses better compared to other distributions. The first percentile of the normal distribution is saved in the memory as the variable L_0 (Figure 3.1.8). Percentile value is also an input parameter for the model; as a result, a user can choose some other percentile values instead of the first percentile.

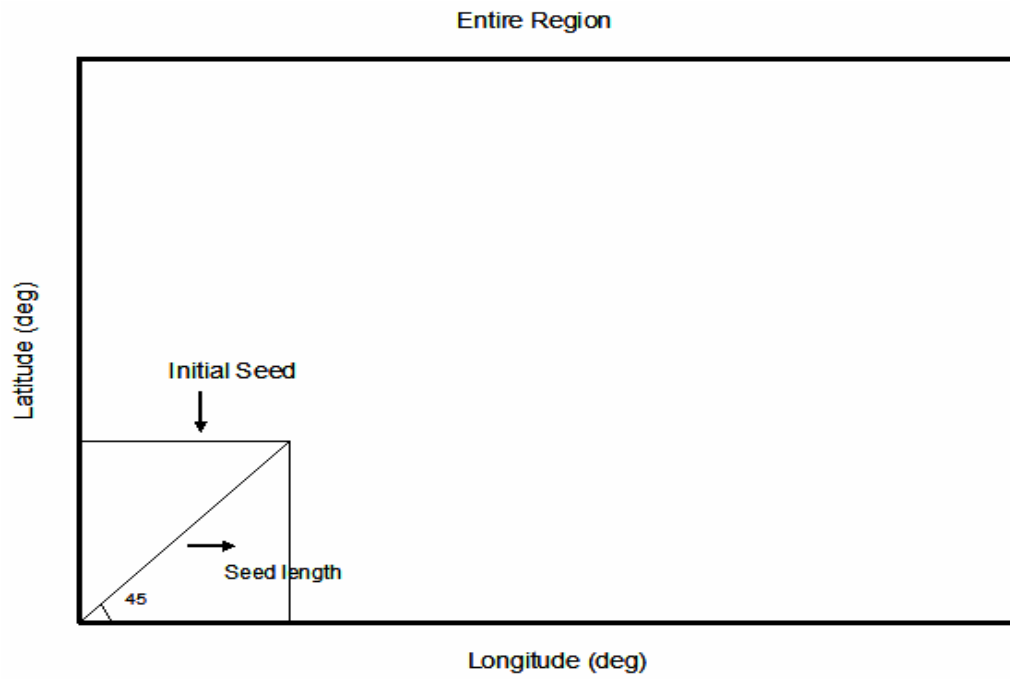


Figure 3.1.7 Initial Seed.

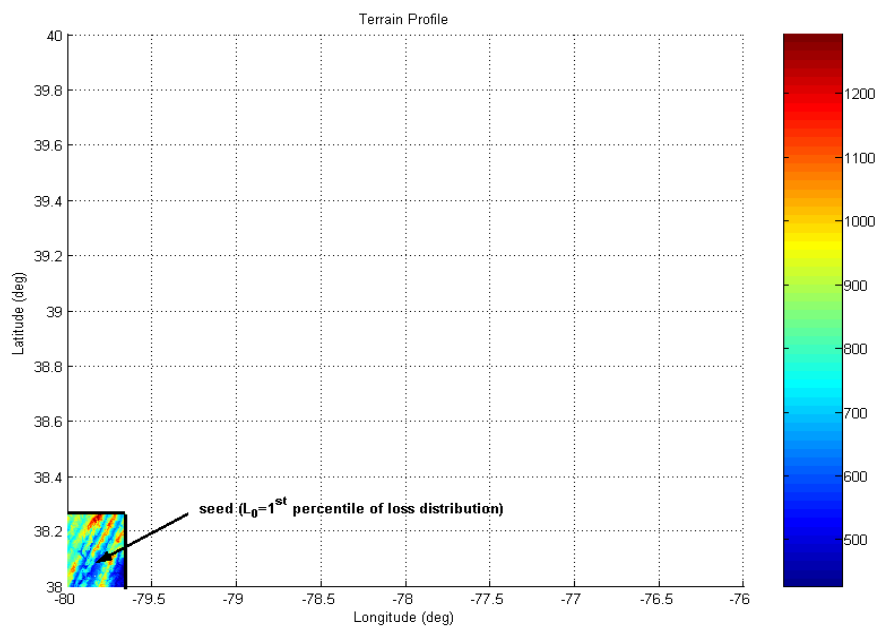


Figure 3.1.8 First Percentile of Loss Distribution for the Initial Seed.

We start to increase the tile length *diagonally* after obtaining the initial seed. Each time the area of the tile is increased, the number of transmitter and receiver pairs and the *maximum distance* between the pairs are also increased. The losses between new transmitter and receiver pairs are again calculated for the new area and the first percentile of the new loss distribution is stored in the memory as the value L . Diagonal growth is stopped if the difference between L and L_o is larger than a user specified value, ϵ_o . This value is equal to 0.01 in our application. The diagonal increase of the tile size is illustrated in Figure 3.1.9.

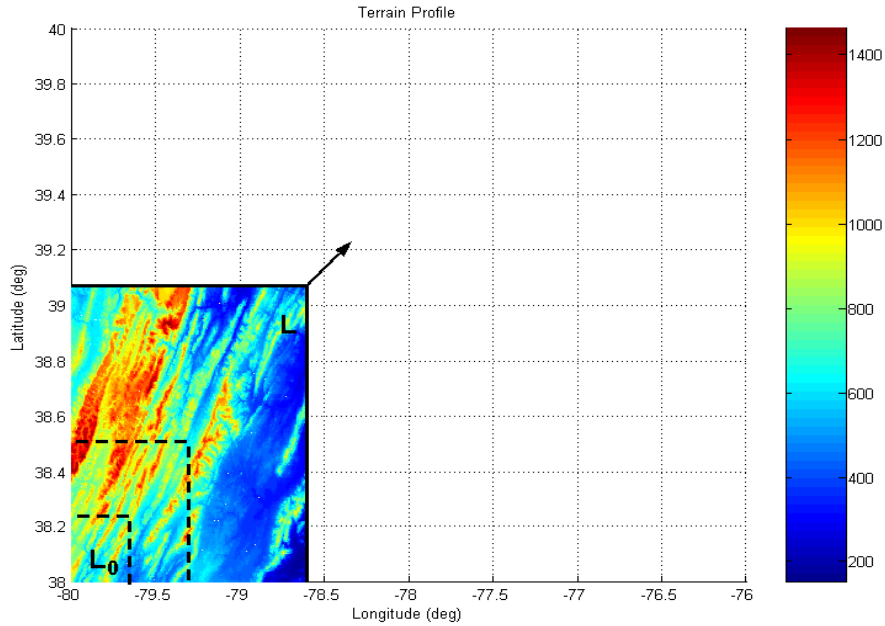


Figure 3.1.9 Diagonal Increase of the Seed Size.

When the difference between L and L_o turns out to be larger than ϵ_o , a *diagonal binary search* is applied to find the optimum seed size (Figure Figure 3.1.10 – Figure 3.1.13). The algorithm is named as *diagonal binary search* since we apply *binary search*

technique when the seed size is increased *diagonally*. It is assumed that the optimum point is in the middle of the previous tile length and the current tile length when $|L - L_0| > \epsilon_0$, thus all the calculations are repeated for the mean tile length while the difference between L and L_0 satisfies the initial criteria, i.e. $|L - L_0| \leq \epsilon_0$.

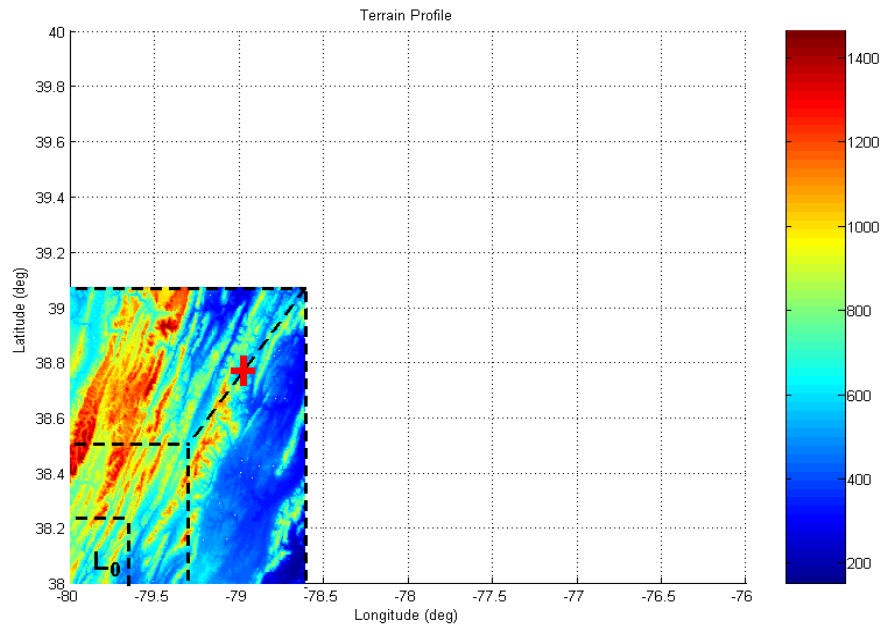


Figure 3.1.10 Diagonal Binary Search – Mean Seed Length is Found.

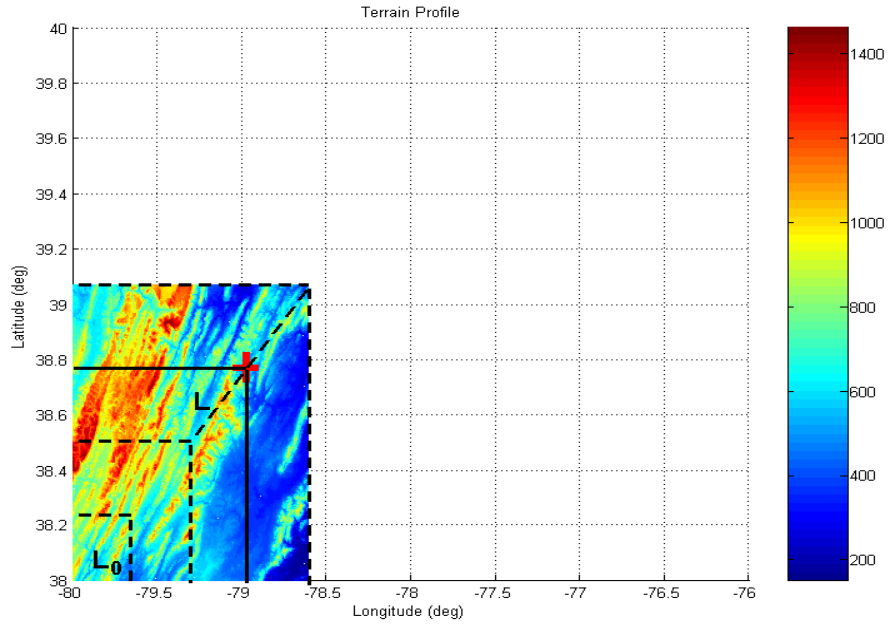


Figure 3.1.11 Diagonal Binary Search – Check the Difference between L and L_0 .

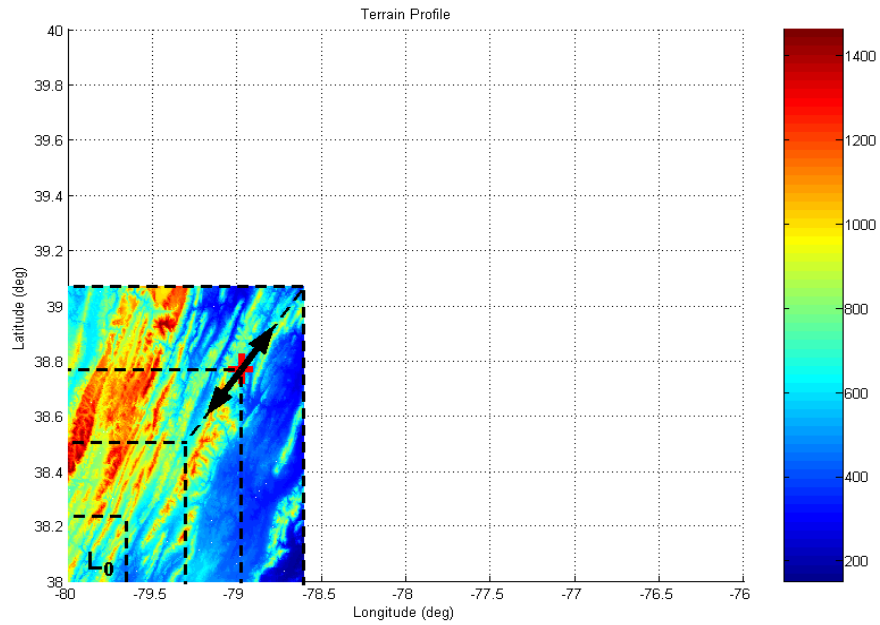


Figure 3.1.12 Diagonal Binary Search – Continue if the Initial Criteria is not Satisfied.

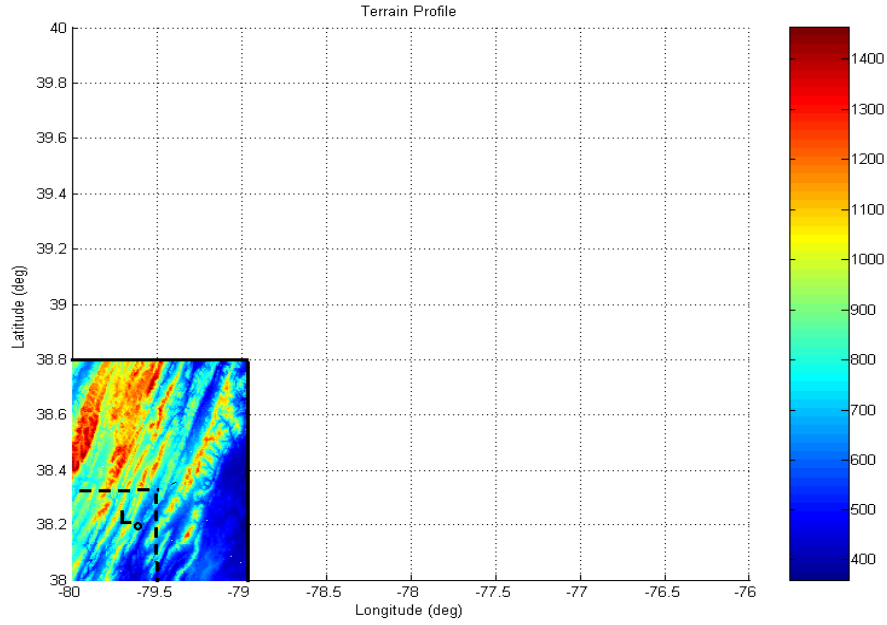


Figure 3.1.13 Diagonal Binary Search – Optimum Seed Size is Determined Diagonally.

The terrain features change dramatically when we keep increasing the area of the seed diagonally at the end of diagonal binary search. At this point, we start to increase the seed size *horizontally*. The seed keeps growing if the characteristic of the area does not differ with fixed latitude and increasing longitude. Basically, we apply the same procedure as we did in diagonal growth – continue to increase the area of the seed horizontally as long as the initial criteria is satisfied such that $|L - L_o| \leq \epsilon_o$ (Figure 3.1.14).

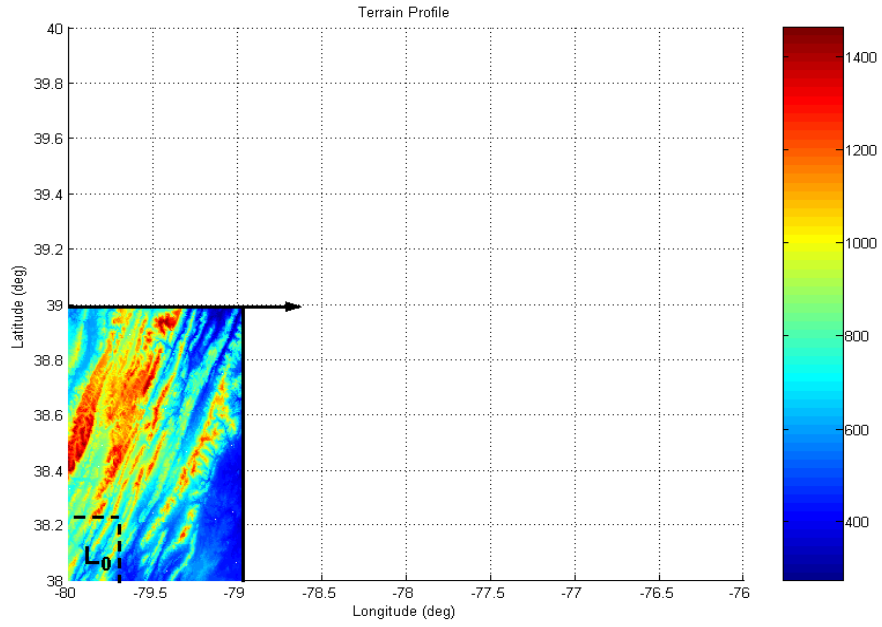


Figure 3.1.14 Horizontal Growth.

Horizontal binary search is applied when the difference between the first percentile values for the previous seed and the current seed exceeds the pre-defined value, ϵ_0 , at the end of horizontal binary search (Figure 3.1.15).

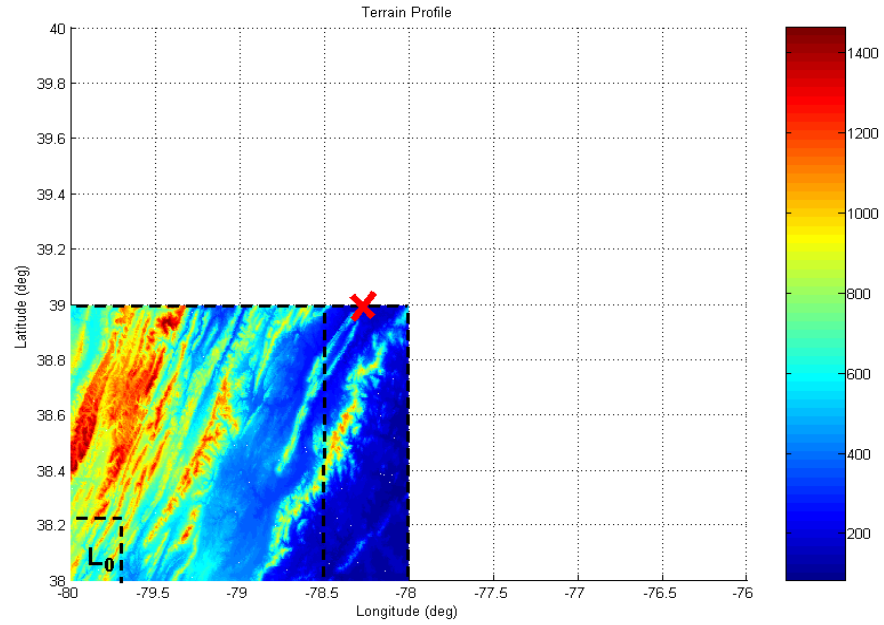


Figure 3.1.15 Horizontal Binary Search.

The optimum longitude value for the sub-area is found at the end of the horizontal binary search. We start to increase the latitude value of the seed at this point. As a result, we start to enlarge the seed *vertically* by increasing the latitude. Figure 3.1.16 illustrates the vertical growth of the seed.

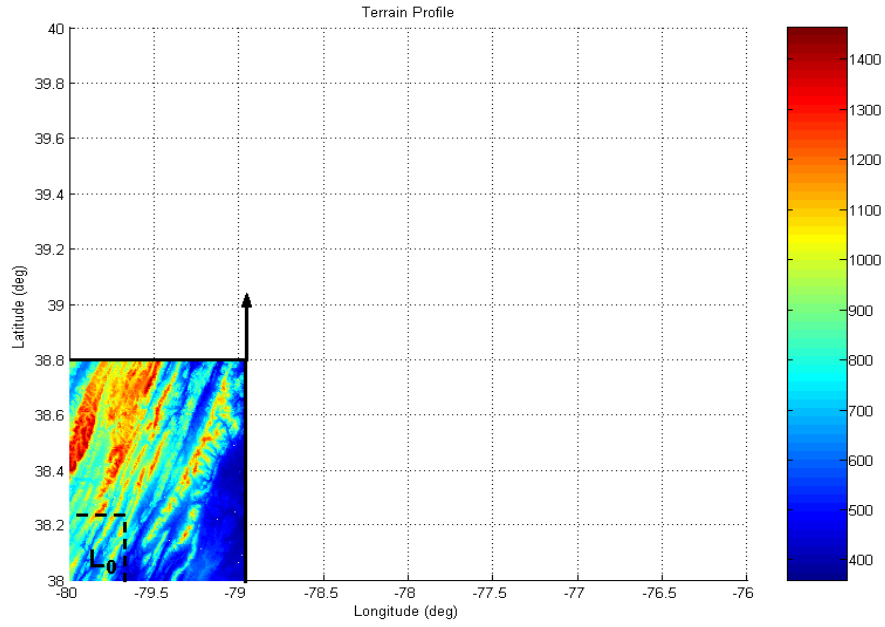


Figure 3.1.16 Vertical Growth.

When the difference between the first percentile value of the previous seed and the current seed is larger than the pre-specified value, ϵ_0 , at the end of vertical growth, we start to apply *vertical binary search* (Figure 3.1.17).

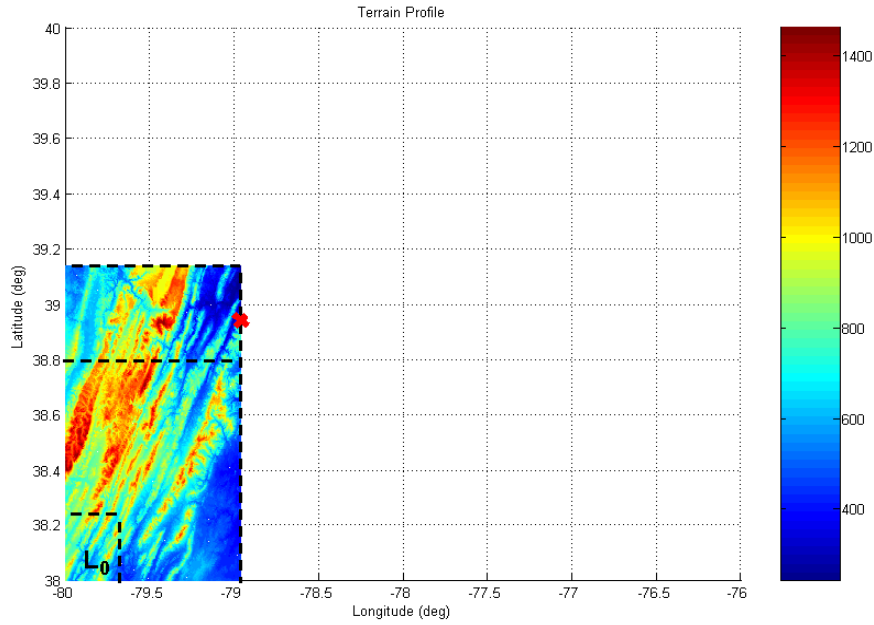


Figure 3.1.17 Vertical Binary Search.

The basic idea of vertical binary search is the same as diagonal and horizontal binary search. The vertical growth stops when the optimum latitude value is found. At the end of all these steps, the first sub-area which has similar terrain features is obtained. In other words, if the tile length for this sub-area is increased further, the pdf of loss distribution will differ dramatically compared to the initial seed.

Tiling the region is continued until the whole area of interest is covered with small sub-areas. Figure 3.1.18 shows the area covered with tiles. Sub-areas do not overlap in Figure 3.1.18 for illustration purposes, but in the real application, sub-areas overlap while tiling the region (Figure 3.1.19). The distances between transmitters and receivers are uniformly distributed between 40 km and 50 km and the transmit frequency is uniformly distributed between 560 MHz and 600 MHz to obtain the tiling in Figure

3.1.19. The start and end points of all the tiles are saved in the memory after the whole region is covered with tiles. The tile which covers a given transmitter or receiver location is determined using saved start and end values of the sub-areas.

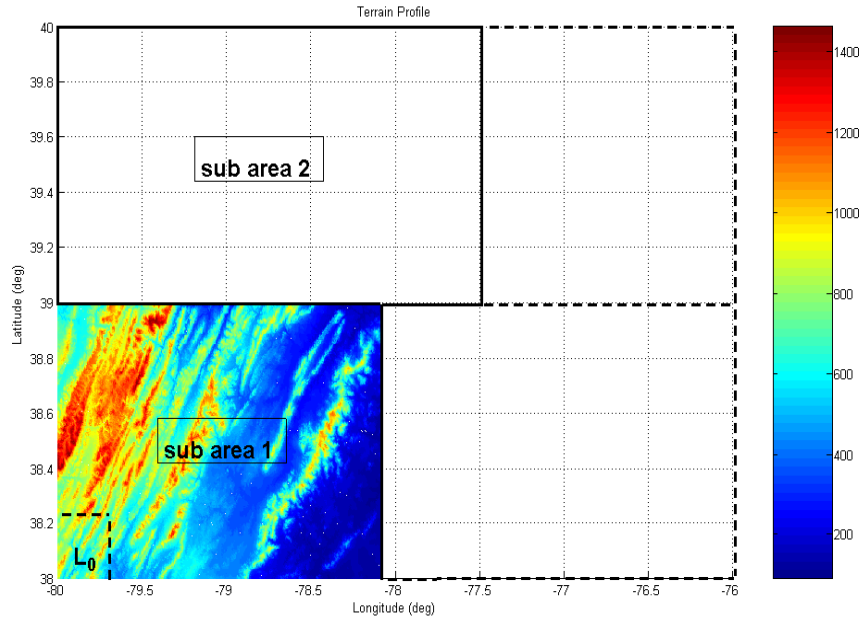


Figure 3.1.18 Tiled Region.

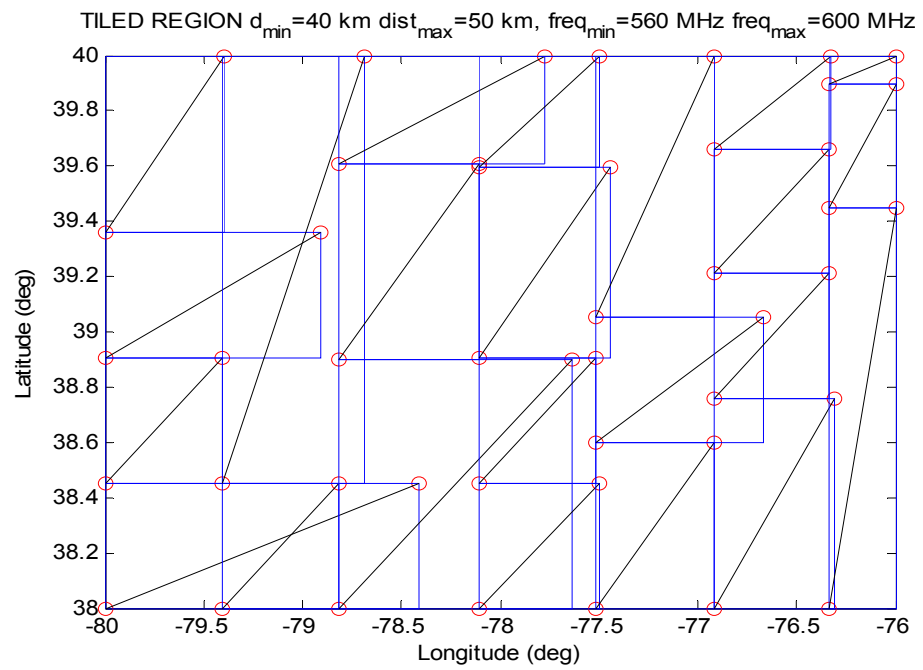


Figure 3.1.19 Tiled Region with Overlapping Sub-areas.

Chapter 4: Application of LPM to Opportunistic Spectrum Access

The application of LPM to opportunistic spectrum access is discussed in this chapter.

4.1 Determining the Percentile of Loss for a Given Transmitter and Receiver

A given area is divided into sub-areas in tiling approach and each tile is assigned a number as shown in Figure 4.1.1.

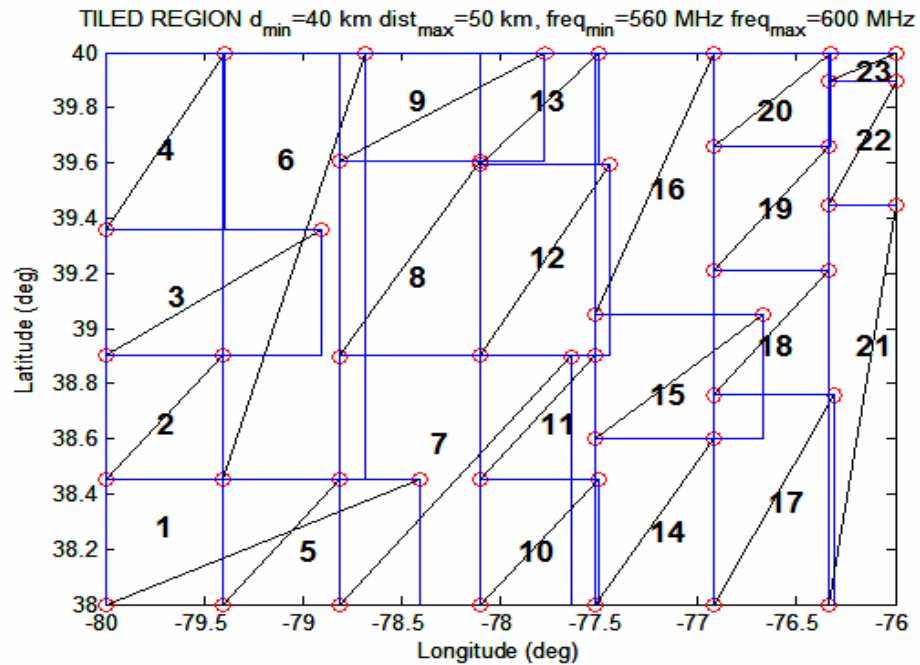


Figure 4.1.1 Numerated Tiles.

A sufficient number of transmitters and receivers proportional to the area size have already been chosen while determining sub-areas in tiling algorithm. Moreover, the corresponding path losses have been calculated. This information was required to obtain the first percentile of pdf of losses, L and L_0 values, during tiling algorithm. Using the same transmitter and receiver locations, distances between transmitter and receivers can be divided into distance bins with a user defined resolution and corresponding loss values can be used to obtain pdf of losses for each distance bin in each tile.

Suppose the user has defined the distances between transmitters and receivers to be uniformly distributed between minimum distance (d_{\min}) and maximum distance (d_{\max}) values for the initial seed of each tile in tiling approach. Maximum distance value is increased during the execution of the code each time the area of the seed is increased diagonally, horizontally or vertically. As a result, each tile has a different maximum distance value at the end. For instance, since there are 23 tiles in the area given in Figure 4.1.1, we can represent each maximum distance value as d_{\max_i} where i represents the tile number which is between 1 and 23. Suppose the user has also specified the distance bin size as Δd . The distances in the same distance bin will be grouped together and the normal pdf of losses will be obtained by using the corresponding losses for each distance value in the bin. In the end, we have n_i number of distributions for every tile and

$$n_i = (d_{\max_i} - d_{\min}) / \Delta d$$

where $1 \leq i \leq 23$.

Table 4.1.1 shows grouping distances into bins for the i^{th} tile.

Table 4.1.1 Grouping Distances into Distance Bins.

<u>Distance Bin</u>	<u>Pdf of Losses</u>
$d_{\min} \rightarrow d_{\min} + \Delta d$	$f_{i,1}(x)$
$d_{\min} + \Delta d \rightarrow d_{\min} + 2\Delta d$	$f_{i,2}(x)$
$d_{\min} + 2\Delta d \rightarrow d_{\min} + 3\Delta d$	$f_{i,3}(x)$
\vdots	\vdots
$d_{\min} + (n_i - 1)\Delta d \rightarrow d_{\max_i}$	$f_{i,n_i}(x)$

Only the mean and the variance values need to be stored in the memory for each normal distribution.

All the above calculations will be done and stored in the memory of DSA devices in advance. As a result, there will not be any loss computation during the use of DSA radios. The DSA nodes will only find the correct tile and corresponding distance bin in the tile to find the mean and the variance value for the loss distribution for that distance bin. As a result, computation time will be short to obtain the path loss. Moreover, with this approach, we overcome the problem of occupying too much memory space while storing detailed terrain information in the memory.

Obtaining the loss value is relatively easy when the transmitter and receiver are in the same tile compared to the case when they are in different tiles. It is enough to take into account the mean and the variance of the loss distribution from the tile that covers

transmitter and receiver when they are in the same tile. Suppose we know the approximate location of a transmitter in an area. We want to calculate the path loss for an approximate distance from the receiver with LPM when the transmitter and receiver are in the same tile.

Figure 4.1.2 shows the case when the transmitter and receiver are in the same tile.

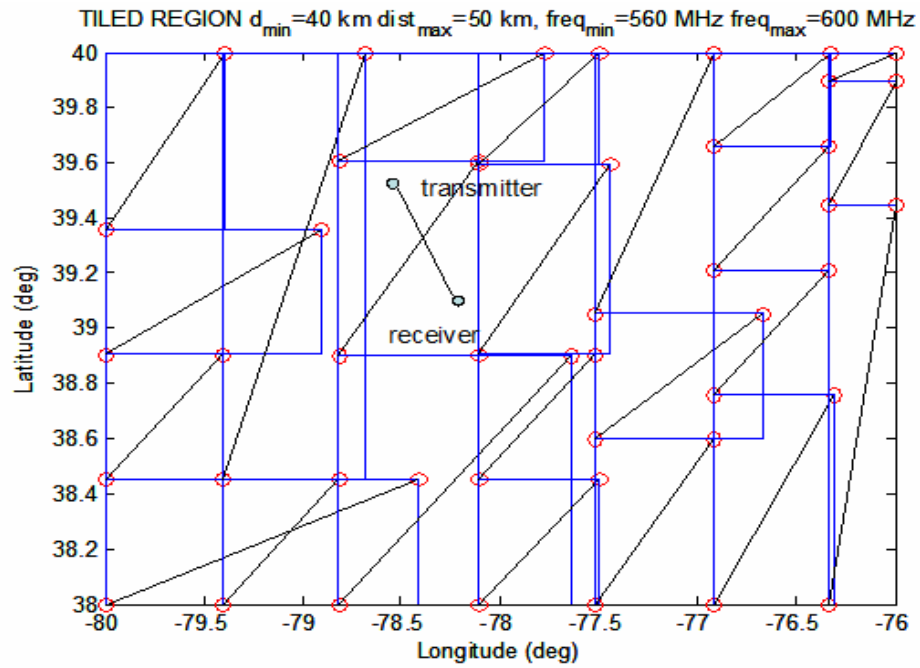


Figure 4.1.2 Transmitter and Receiver Pair in the Same Tile.

First, the tile which covers the given transmitter is found. For instance, the transmitter and receiver are in the 8th tile (see Figure 4.1.1) in Figure 4.1.2. Then, the distance bin which contains the distance between the transmitter and receiver is determined in the corresponding tile. The mean and the variance of the loss distribution for the given distance bin is retrieved from the memory. Then, the user can choose the

percentile value and obtain the path loss for that percentile. The value used as *percentile* depends on the information the user has about the location of the transmitter and receiver. Lower percentile values, i.e. 1st percentile, should be chosen to decrease the probability of interference if the user does not have enough information about the locations.

Equation 4.1.1 gives the formula used to calculate the specified percentile of loss, *percentile*, using the mean, μ , and variance, σ^2 of the normal distribution.

Equation 4.1.1.

$$L = \mu - \sigma * \text{inv}Q\left(\frac{\text{percentile}}{100}\right)$$

where $Q(x) = \frac{1}{\sqrt{2\Pi}} \int_x^{\infty} e^{-\frac{t^2}{2}} dt$.

On the other hand, if the transmitter and receiver pairs are in different tiles, the mean and variance of the loss distribution is found considering the mean and variance of the loss distribution from all the tiles between the given transmitter and receiver.

If the distance between a given transmitter and receiver is shown as d and each portion of line d in different tiles is represented as d_i , then

Equation 4.1.2

$$d = d_1 + d_2 + \dots + d_i + \dots + d_n$$

where d_1 is the portion of the line between transmitter and receiver in the tile which contains the transmitter, and d_n is the portion of the line in the tile which contains the receiver (Figure 4.1.3).

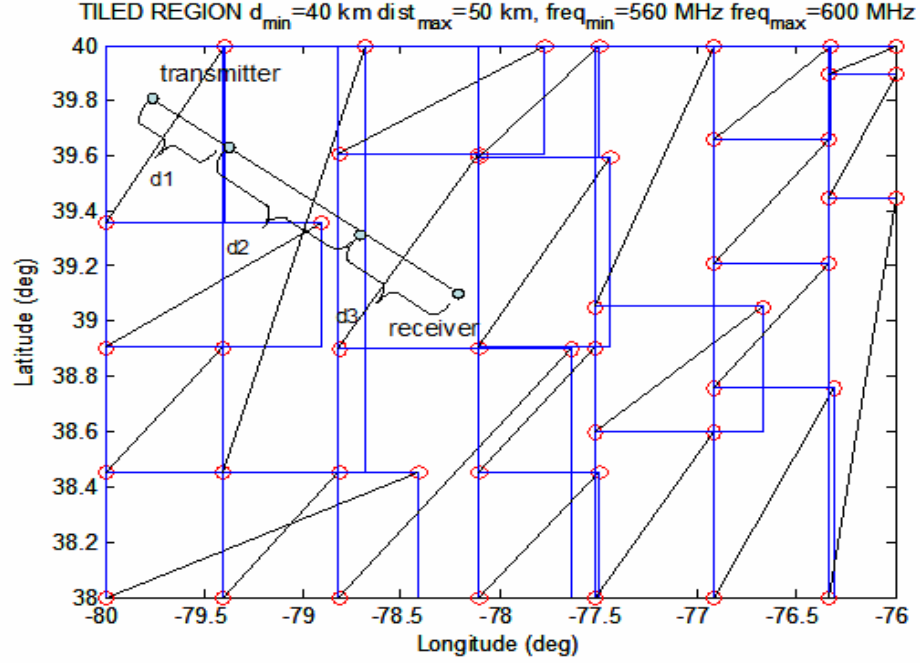


Figure 4.1.3 Transmitter and Receiver Pair in Different Tiles.

The sum of normal distributed variables has also a normal distribution. We use this property of normal distribution when we combine loss data from different tiles when the transmitter and receiver are in different tiles. If the mean and the variance of the individual tiles are shown as μ_i and σ_i^2 , respectively, when transmitter and receiver are in different tiles the mean and variance of the distribution of losses are given by:

Equation 4.1.3

$$\mu = (d_1/d) * \mu_1 + (d_2/d) * \mu_2 + \dots + (d_i/d) * \mu_i + \dots + (d_n/d) * \mu_n$$

$$\sigma^2 = (d_1/d)^2 * \sigma_1^2 + (d_2/d)^2 * \sigma_2^2 + \dots + (d_i/d)^2 * \sigma_i^2 + \dots + (d_n/d)^2 * \sigma_n^2$$

The specified percentile of loss is again calculated using Equation 4.1.1 with the mean and variance values obtained in Equation 4.1.3.

4.2 Using LPM to Determine MIFTP

Maximum Interference Free Transmit Power (MIFTP) is the maximum transmit power level a DSA device can use without causing harmful interference to the legacy user receivers. The LPM approach is very useful when determining the MIFTP for a DSA device since one can determine a path loss value without using the exact locations of transmitter and receiver. The interference range for legacy user receivers can be calculated and the transmit power level of the DSA devices can be adjusted using this path loss value.

The pdf of losses for the untiled region can be used when there is no information about either the location of the transmitter or the receiver. Choosing lower percentiles of pdf of losses will be more appropriate in this case. For the cases when we at least know the approximate location of either the transmitter or receiver, we can use the pdf of losses for the tiled region by retrieving the loss data from the appropriate tiles. If there are lots of obstacles which will cause absorption in the area, higher percentile losses can be used (i.e., 10%), but if the transmitters and receivers are in an open area, then the path loss will be small and the received signal level at the non-cooperative node receiver will be high.

Thus, it will be more appropriate to use lower percentiles of loss distributions (i.e., 1%) in an open area.

Chapter 5: Performance Evaluation of LPM

Three criteria are considered to evaluate the performance of the LPM path loss model: memory requirement, violation probability and calculation time.

5.1 Memory Requirement

Probability density functions of losses are obtained for every distance bin in each tile while using LPM. Thus, the number of pdf of losses saved for each tile differs depending on the resolution chosen while grouping the distances. The number of pdf of losses saved also depends on the number of tiles in the area. If the terrain characteristics differ dramatically in the given area, the number of tiles and the amount of data to be saved will increase. For instance, DSA devices are planned to be used all over the U.S.; as a result, the data for the map of whole country would have to be saved in the memory of each DSA device for each tile. The required memory with LPM would be very large in this case. We tried to overcome this problem by converting the non-parametric distribution of losses to normal distribution and saving only the mean and the variance in the memory for each distance bin in each tile.

While generating the LPM path loss model, we worked with a relatively small area, with a size of 222 km x 350 km. There are 23 tiles in the tiled region in Figure 4.1.1, and the required memory to save the parameters of normal distribution and start

and end points for all the tiles and input parameters are 96 kbytes. However, the required memory space to store the terrain data with TIREM model for the same area is 1.38 Mbytes. As a result, LPM model requires very small memory space compared to TIREM model. Moreover, the memory requirement can be decreased further in LPM by increasing the resolution of the distance bins and the size of each tile depending on the application by adjusting the ϵ_0 value, i.e. stop increasing the area of the tile when $|L - L_0| > \epsilon_0 = 0.1$ instead of $|L - L_0| > \epsilon_0 = 0.01$.

5.2 Violation Probability

One other criteria considered while evaluating LPM is violation probability. The path loss values from TIREM model are accepted as truth and ‘violation’ is defined as the time the first percentile of the pdf of losses from LPM model exceed the loss value obtained using the TIREM model, i.e. $L_{LPM} > L_{TIREM}$. The results from both untiled and tiled regions are considered while calculating the violation probability and the results are given in this section.

For the untiled region, the violation probability is 0.04% for 2500 samples. On the other hand, violation probability is 0.72% for 2500 samples for tiled region. LPM loss value is 2 or 3 dB higher than the one for TIREM model for most of the violation cases. The mean of the difference between TIREM model path loss and LPM path loss is (48.3 ± 0.01) dB with a 95% confidence level. As a result, violation probability is less than 1% with LPM and the impact of the interference will not be very high compared to

TIREM model even in the case of interference since there is not a big difference between path loss values when violation occurs.

5.3 Calculation Time

TIREM model takes the locations of transmitter and receiver and detailed terrain data as input parameters and gives the path loss value as output. On the other hand, all the loss calculations are done in advance with LPM and the mean and variance values of the loss distributions of each distance bin in each tile are saved in the memory. In other words, instead of calculating path loss, LPM model retrieves the path loss data from the memory. As a result, it is expected that LPM model takes less time compared to TIREM model.

The number of tiles between the transmitter and receiver affects the calculation time for LPM. For instance, in Figure 5.3.1, several tiles has to be gone through and mean and variance of the loss distribution in those tiles for the corresponding distance bins has to be considered in order to find the final path loss with LPM. On the other hand, checking the loss distribution of only one tile is enough for Figure 5.3.2 since the transmitter and receiver are in the same tile.

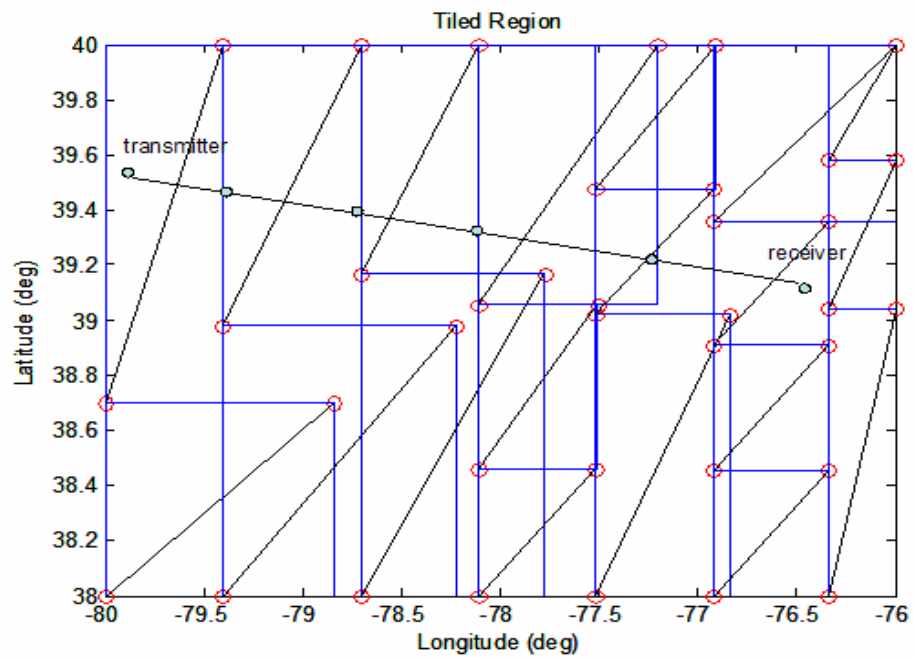


Figure 5.3.1 A Given Transmitter and Receiver Far Away From Each Other.

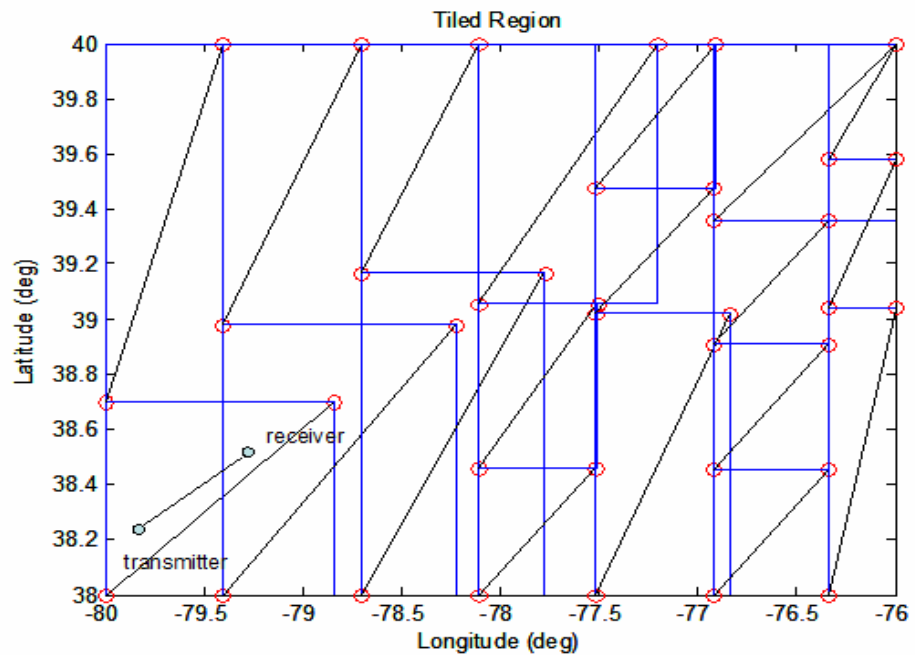


Figure 5.3.2 A Given Transmitter and Receiver Close to Each Other.

MATLAB is used for LPM, and TIREM model is written in the C language. Moreover, some 'for' loops have to be used in MATLAB code while calculating path losses with LPM. As a result, this increases the calculation time for LPM and it is not a fair comparison to compare the execution time for TIREM and LPM in two different programming environments. However, since path loss calculations are done in advance with LPM model, the TIREM model should take more time compared to LPM if they were implemented using the same programming language.

Chapter 6: Spectrum Sensing via the Multitaper Method

A new approach to determine the MIFTP more accurately is explained in Chapter 3 through Chapter 5. However, DSA devices need to sense the channel and determine that the signal level is below a threshold value at that frequency in a certain time and location before starting to use the channel and determining MIFTP.

A spectrum hole can be defined as a frequency band that is not being used by a primary user at a particular time and geographic region [10] and as mentioned before, spectrum sharing can be performed by DSA nodes, which have the capability of dynamically tuning to spectrum holes within a frequency range. To determine the spectrum holes accurately, a DSA node should be equipped with a highly sensitive detector and an algorithm to access the unused spectrum without causing harmful interference to the primary users of the spectrum. In this section, the multitaper (MT) spectral estimation method is applied to the problem of spectrum sensing in TV bands and the performance of the MT method is compared with that of conventional FFT-based spectrum estimation [11].

6.1 Spectral Estimation

Spectrum holes are determined by examining the power spectral density of the received signal. Therefore, accurate and efficient methods of power spectral estimation are required to determine the spectrum holes.

In [12], ultra-sensitive TV detector measurements are analyzed using the conventional FFT-based method. The MT method was introduced by Thomson [13] and has been shown to have superior performance in some applications such as geoclimate sensing [14]. Haykin [1] suggests that the multitaper method would be effective in spectrum sharing applications, but we are not aware of empirical studies applying the multitaper method to spectrum hole detection using real measurement data. In [12], the conventional FFT method is used to study TV detector measurement data. In this chapter, we compare the performance of the FFT method versus the MT method with respect to spectrum sensing using the empirical TV measurement data from [12].

6.1.1 Conventional FFT Method

Given a time series, $\{X_1, X_2, \dots, X_N\}$, the conventional FFT method estimates the power spectral density $S(\cdot)$ as follows:

Equation 6.1.1

$$S^{fft}(f) = \frac{\Delta t}{N} \left| \sum_{t=1}^N X_t e^{-j2\pi f t \Delta t} \right|^2,$$

where Δt is the spacing between the samples. The function $S^{fft}(f)$ is known as the periodogram [15]. The periodogram is an unbiased estimate of the power spectral density for white Gaussian noise, but its variance is equal to a constant that is independent of the data length N . As a result, $Var[S^{fft}(f)] \neq 0$ as $N \rightarrow \infty$. Hence, the periodogram is an inconsistent estimator of the power spectrum [15].

6.1.2 Multitaper Method

Multitaper spectral analysis is a method for spectral estimation of a time series that is believed to exhibit a spectrum containing both continuous and singular components. This method involves the use of a set of K orthogonal tapers, called Discrete Prolate Spheroidal Sequence (DPSS) tapers. K represents the tradeoff between resolution and the variance properties of the spectral estimate. The variance of the spectral estimate can be decreased when K is large. On the other hand, we smear out the fine features and decrease the resolution of the spectral estimate by increasing the value of K . The k^{th} taper is a sequence $\{h_{t,k} : t = 0, 1, \dots, N\}$. Each taper provides protection against spectral leakage [13]. The time series data is windowed with each of the K DPSS tapers and then a periodogram is computed via the FFT [15]. The high resolution multitaper spectrum is a weighted sum of K eigenspectra, $\hat{S}_k^{mt}(\cdot), k = 0, \dots, K-1$ (see [16], p. 369):

Equation 6.1.2

$$S^{mt}(f) = \frac{\sum_{k=0}^{K-1} \lambda_k \hat{S}_k^{mt}(f)}{\sum_{k=0}^{K-1} \lambda_k},$$

where

$$\hat{S}_k^{mt}(f) = \Delta t \left| \sum_{t=1}^N h_{t,k} X_t e^{-j2\pi f t \Delta t} \right|^2,$$

$h_{t,k}$ is the t^{th} DPSS taper element for the k^{th} direct spectral estimator $\hat{S}_k^{mt}(\cdot)$, and λ_k is the eigenvalue corresponding to the eigenvector with elements $\{h_{t,k}\}$ (see [16], p. 103).

A more leakage-resistant spectral estimate, called an adaptively weighted multitaper (AWMT) spectrum, can be obtained by adjusting the relative weights on the contributions from each of the K eigenspectra as follows (see [16], p. 370):

Equation 6.1.3

$$S^{amt}(f) = \frac{\sum_{k=0}^{K-1} b_k^2(f) \lambda_k \hat{S}_k^{mt}(f)}{\sum_{k=0}^{K-1} b_k^2(f) \lambda_k}$$

where $b_k(f)$ is a weighting function that further guards against broadband leakage for a non-white (“colored”) but locally-white process. The weight of the k^{th} eigenspectrum is proportional to $b_k^2(f) \lambda_k$, where

$$b_k(f) = \frac{S(f)}{\lambda_k S(f) + (1 - \lambda_k) \sigma^2 \Delta t}.$$

Parseval's theorem is satisfied in expected value in Equation 6.1.2, because the weights in the estimator do not depend on the frequency. On the other hand, the AWMT spectral estimator given in Equation 6.1.3 generally does not satisfy Parseval's theorem in expected value [16].

6.2 Numerical Results

Spectrum measurements were made at a residential location in McLean, Virginia¹. The equipment was connected to a standard TV antenna located on the second story roof. The measurement data consists of time series data collected over a period of approximately 8 minutes for 40 different starting times. Thus, we have a collection of $M = 40$ sets of time series data available to us, which we represent by $\{X_t^{(i)}\}$, where $X_t^{(i)}$ denotes the t^{th} sample in the i^{th} data set with $i = 1, \dots, M$ and $t = 1, \dots, N$, where $N = 819,200$. The time spacing between samples is $\Delta t = 0.586$ ms.

Figure 6.2.1 and Figure 6.2.2 show three types of graphs corresponding to the FFT and MT methods, respectively:

- a) maximum hold (max-hold) plot,
- b) waterfall plot,
- c) duty cycle plot.

¹ The measurements were taken by Shared Spectrum Company.

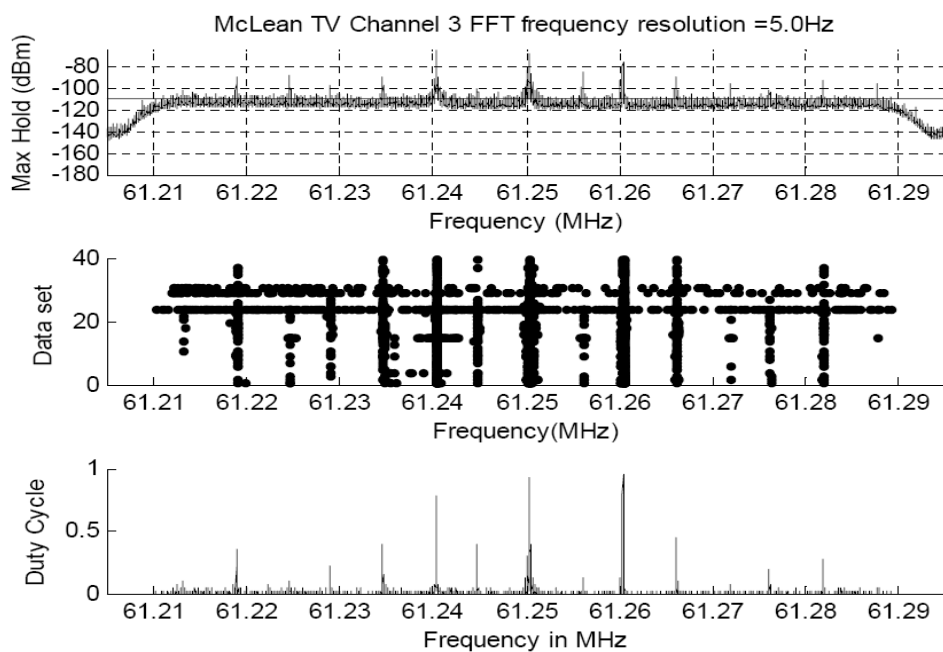


Figure 6.2.1 Max-Hold Plot for TV Channel 3 Using the FFT Method.

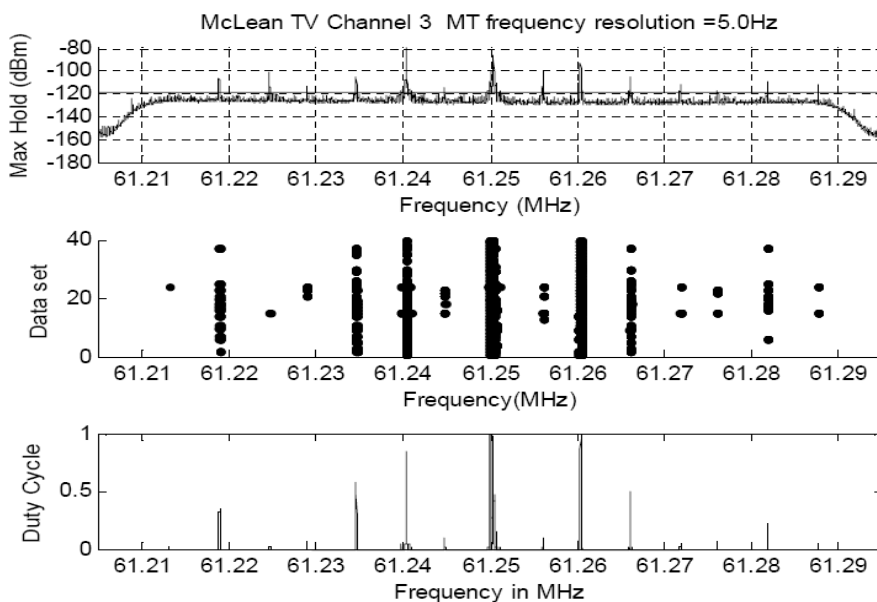


Figure 6.2.2 Max-Hold Plot for TV Channel 3 Using the MT Method.

Both the standard MT and the AWMT methods are applied to the data and no significant difference is observed in the results. The results presented in this thesis are obtained using AWMT method with $K = 7$ tapers.

Let $S_i(f)$ denote the spectral estimate obtained from the first $N = 18,000$ samples of the i^{th} data set or time series (using the FFT method or the MT method). The max-hold power spectral estimate is defined by

Equation 6.2.1

$$S_{mh}(f) = \max_{1 \leq i \leq M} S_i(f), \quad f_l \leq f \leq f_h,$$

where $f_l = 61.2$ MHz and $f_h = 61.3$ MHz. The waterfall plot shows the set of points (f, i) , for which the spectral estimate $S_i(f)$ exceeds a given threshold η over the M data sets. The set of points in the waterfall plot can be expressed as

Equation 6.2.2

$$W = \{(f, i) : S_i(f) \geq \eta, 1 \leq i \leq M, f_l \leq f \leq f_h\}.$$

The duty cycle plot shows, for each frequency f , the proportion of data sets for which $S_i(f)$ exceeds the threshold η . In other words, the value of the duty cycle plot at the frequency value f is given by

Equation 6.2.3

$$d(f) \stackrel{\Delta}{=} \frac{1}{M} \sum_{i=1}^M 1_{\{s_i(f) \geq \eta\}}, \quad f_l \leq f \leq f_h,$$

where 1_A denotes the indicator function on the set A . Thus, the duty cycle plot renders negligible spectral components that have high power for only a small number of data sets.

For the waterfall and duty cycle plots in Figure 6.2.1 and Figure 6.2.2, detector threshold values of $\eta = -110$ dBm and $\eta = -119$ dBm were used, respectively. Comparing these two figures, we can make the following qualitative observations. From the maxhold plots, we see a smaller variation in the spectral estimates obtained via the MT method. The average signal level in the max-hold plot is lower in the case of the MT method, since it is able to suppress more of the noise components. From the waterfall plots, we see that the MT method removes misleading information. From the duty cycle plots obtained using the MT method, we can much more easily identify the carrier signal and the synchronization pulses, which are 15 kHz apart from each other in each channel. The duty cycle plots can be used to determine whether a channel is free or occupied at a specific time.

The performance curves shown in Figure 6.2.3 through Figure 6.2.6 were obtained using duty cycle plots for which the detector threshold value η was varied from -120 to 0 dBm. To obtain these figures, power spectrum estimates corresponding to each of the $M = 40$ data sets were computed using the first $N = 1500$ samples from each set. Note that this number of samples corresponds to a time period of approximately 35

seconds. Then duty cycle values are computed using Equation 6.2.3 for a given value of η .

Figure 6.2.3 shows the number of correctly identified busy channels versus the threshold level for both the FFT method and the MT method. A channel is identified as busy (i.e., a signal is present) if the duty cycle value $d(f)$ corresponding to the carrier frequency exceeds a threshold of 0.2 (i.e., 20%). Using a threshold value of 0.2 provides an adequate probability of detection and probability of false alarm. In the MT method, the noise components of the signal and the variance of the spectral estimate are reduced such that the power of the MT-based estimate is less than that of the FFT-based estimate. As a result, the number of detected channels is higher for the FFT method when the threshold level is between -70 dB and -30 dB. However, in practice, such high values would not be used as a detector threshold; opportunistic spectrum access requires much lower detector thresholds. The objective here is to decrease the threshold as much as possible in order to obtain accurate information about spectrum occupancy.

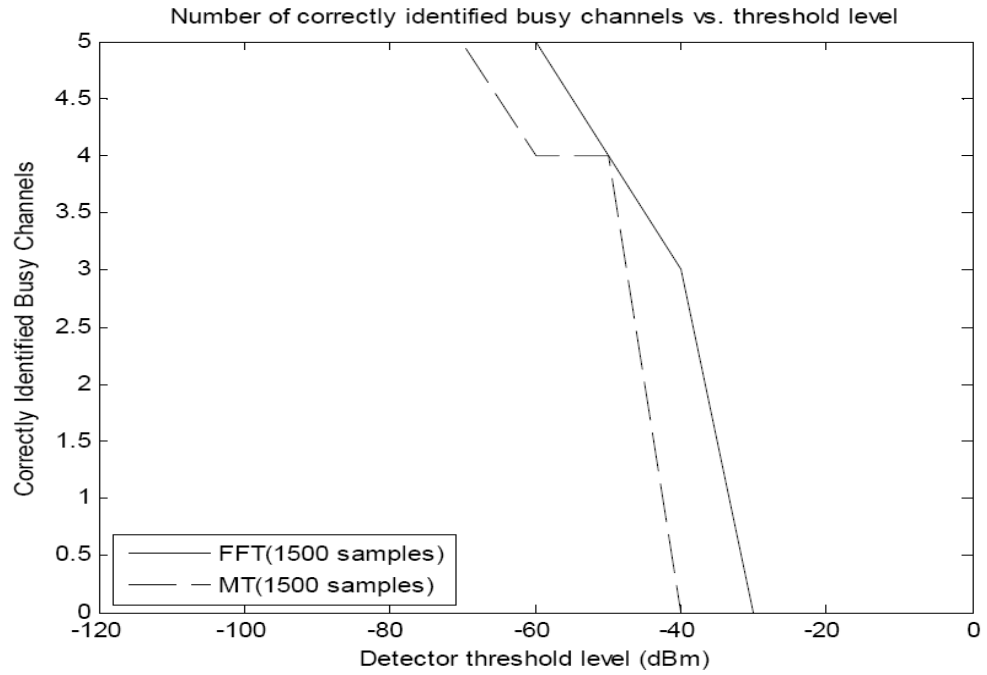


Figure 6.2.3 Number of correctly identified busy channels vs. Threshold Value.

Figure 6.2.4 shows the number of *false alarm* channels versus the detector threshold level. A false alarm channel refers to a channel that is identified as busy, when it is actually free. We observe that the number of false alarm channels is lower for the MT method when the threshold level is between -120 and -80 dBm.

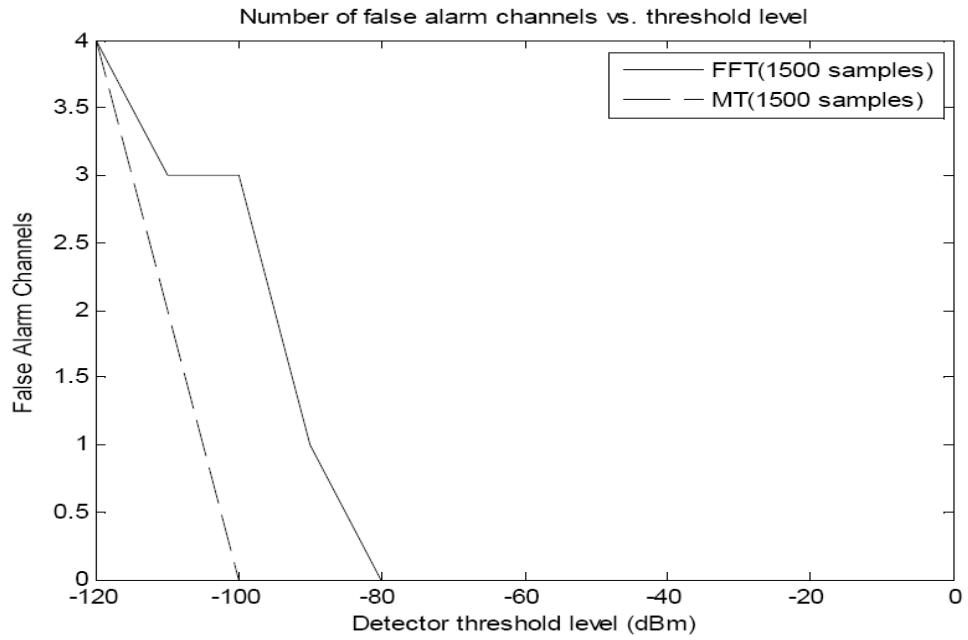


Figure 6.2.4 Number of False Alarm Channels vs. Threshold Value.

Figure 6.2.5 shows the number of miss-detected channels versus the detector threshold. A *miss-detected* channel refers to a channel that is identified as free, when it is actually busy. The number of miss-detected channels is the same for both MT and FFT methods for the threshold levels of interest.

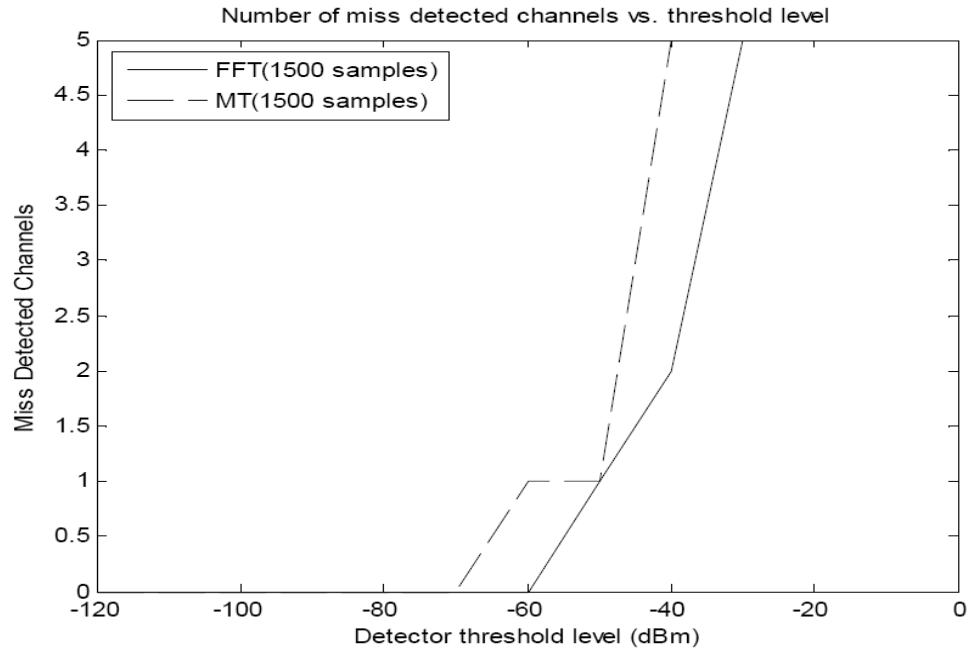


Figure 6.2.5 Number of Miss-Detected Channels vs. Threshold Value.

Figure 6.2.6 shows the number of correctly identified free channels versus the detector threshold. The correctly identified free channels represent the channels that are available for spectrum sharing. The number of correctly identified free channels is higher with MT method between -120 and -80 dBm. If we set a fixed threshold level, e.g. -100 dB and examine the statistics using this threshold level, we can see that the number of correctly identified busy channels and the number of miss-detected channels are the same for both methods. On the other hand, the number of false alarm channels is lower and the number of correctly identified free channels is higher for the MT method. Thus, we see that more channels can be harvested by means of the MT method compared with the FFT method, using a lower threshold level.

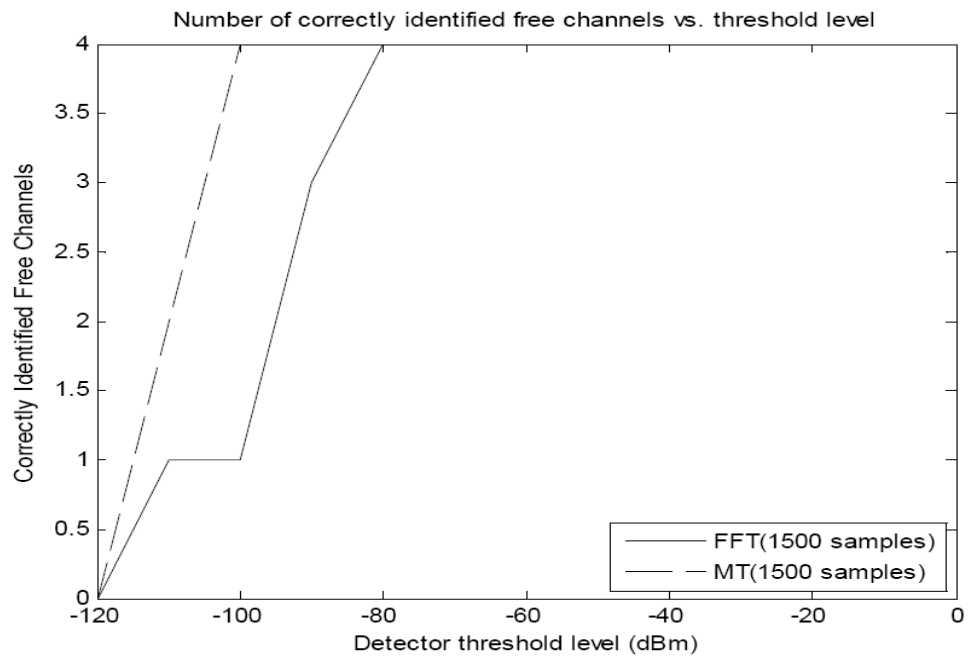


Figure 6.2.6 Number of Correctly Identified Free Channels vs. Threshold Value.

Chapter 7: Conclusion

A novel path loss model, Location Based Propagation Modeling, based on the existing TIREM model is developed in this thesis. The model divides a given region into sub-areas based on user defined criteria and gives the probability density functions of path losses for different distance bins in each sub-area. Only the mean and the variance of losses are saved in the memory after obtaining the pdfs of losses. As a result, detailed terrain information does not need to be saved in the memory to calculate the path losses. Moreover, LPM does not require precise locations of transmitter and receiver as input parameters. This feature of LPM makes it very useful for spectrum sharing applications.

The memory requirement, computation time and violation probability are considered in evaluating the performance of the LPM path loss model. The memory requirement for LPM is less compared to the TIREM model since all the path loss calculations are done in advance and the mean and variance of pdf of losses are saved in the database. The amount of data to be saved depends on the number of tiles and number of distance bins in each tile since there is a loss distribution for each tile. For instance, when the region of interest gets bigger, it is highly probable that the difference between the terrain characteristics will increase. Thus, the number of tiles will increase. The LPM model overcomes the memory problem by saving only the mean and the variance values for distribution of losses for every distance bin in each tile.

The violation probability is given for both tiled and untiled regions in Chapter 5. The violation probability is less than 1% and the path loss values are only 2 or 3 dB higher than the loss from TIREM model in the violation cases.

It is expected that LPM model will be faster compared to TIREM model since all the path loss calculations are completed offline and the data is stored in the memory in LPM. With LPM, time is required to retrieve the data from the memory other than calculating the path losses from the beginning. The code for LPM was written using MATLAB and C language is used for TIREM model. As a result, it is not a fair comparison to compare the calculation time for LPM and TIREM models using MATLAB.

When the number of transmitter and receiver pairs chosen is not sufficient for the initial seed, the size of tiles changes in every execution of the code for a given area. A large number of samples should be used for each tile for the tiling to be consistent in different executions of the code. In other words, we should be able to obtain the same tiling for a given area regardless of the number of samples chosen. This will increase the memory requirement, but give more stable results in the mean time. A database with enough number of samples in each tile will be formed for bigger areas in ongoing work.

We mostly concentrated on determining MIFTP in this thesis, but localization is also an important problem in spectrum sharing applications. The aim is to determine the location of a receiver for a given transmit power and distance with localization. The path loss model used is again very important in localization problem especially if the DSA device uses a high transmit power.

The application of the multitaper method of spectral estimation to the problem of spectrum harvesting in TV bands is also discussed in this thesis. It is known that the computational complexity of the MT method is greater than that of the FFT method by a factor of K , where K is the number of tapers used. However, for relatively small time series, e.g., 1500 samples taken over 40 different data sets amounts to about 35 seconds, the MT method is fast enough to be used in real-time. The performance of spectrum harvesting using the conventional FFT method versus the MT method is compared using empirical TV measurement data and the noise reduction properties of the MT method relative to the FFT method are observed qualitatively from the max-hold, waterfall, and duty cycle plots. The preliminary results with TV measurement data indicate that the noise reduction property of the MT method can result in a significant gain in the number of correctly identified free channels compared to the FFT method. This suggests that significant gains in spectrum harvesting may be achievable in more general settings. In ongoing work, the MT method will be applied to larger sets of measurement data from a variety of signal sources.

BIBLIOGRAPHY

BIBLIOGRAPHY

- [1] S. Haykin, "Cognitive Radio: Brain-Empowered Wireless Communications," IEEE J. Selected Areas in Comm., vol. 23, pp. 201–220, Feb. 2005.
- [2] A. E. Leu, M. McHenry, and B. L. Mark, "Modeling and analysis of interference in listen-before-talk spectrum access schemes," Int. J. Network Mgmt, vol. 16, pp. 131–147, 2006.
- [3] Zhu Ji, K. J. Ray Liu, "Dynamic Spectrum Sharing: A Game Theoretical Overview," in IEEE Communications Magazine, May 2007.
- [4] Mohammad Ghavami, L. B. Michael, Ryuji Kohno, "Ultra Wideband Signals and Systems in Communication Engineering," John Wiley & Sons, January 2005.
- [5] M.N. Lustgarten, James A. Madison, "An Empirical Propagation Model (EPM - 73)," in IEEE Transactions on Electromagnetic Compatibility, Vol. EMC-19, No. 3, August 1977.
- [6] Jon W. Mark, Weihua Zhuang, "Wireless Communications and Networking," Prentice Hall, 2003.
- [7] Federal Communications Commission, www.fcc.gov/Bureaus/Engineering-Technology/Documents/bulletins/oet69/oet69.pdf
- [8] IEEE Vehicular Technology Society Committee on Radio Propagation, "Coverage Prediction for Mobile Radio Systems Operating in the 800/900 MHz Frequency Range," in IEEE Transactions on Vehicular Technology, Vol. 31, No. 1, February 1988.
- [9] Alion Science and Technology Corporation, <http://www.alionscience.com>.
- [10] P. Kolodzy, "Next generation communications: Kickoff meeting," in Proc. DARPA, October 2001.
- [11] T. Erpek, A. E. Leu, and B. L. Mark, "Spectrum Sensing Performance in TV Bands Using the Multitaper Method," IEEE 15th Signal Processing and Communications Applications, 2007.

- [12] A. E. Leu, K. Steadman, M. McHenry, and J. Bates, "Ultra Sensitive TV Detector Measurements," in Proc. IEEE Int. Symp. on New Frontiers in Dynamic Spectrum Access Networks (DySPAN), pp. 30–36, Nov. 2005.
- [13] D. J. Thomson, "Spectrum Estimation and Harmonic Analysis," Proc. IEEE, vol. 70, pp. 1055–1096, September 1982.
- [14] M. E. Mann and J. Park, "Oscillatory spatiotemporal signal detection in climate studies: A multiple-taper spectral domain approach," Advances in Geophysics, vol. 41, pp. 1–131, 1999.
- [15] T. P. Bronez, "On the Performance Advantage of Multitaper Spectral Analysis," IEEE Trans. on Signal Proc., vol. 40, pp. 2941–2946, December 1992.
- [16] D. B. Percival and A. T. Walden, "Spectral Analysis for Physical Applications," Cambridge University Press, 1993.

CURRICULUM VITAE

Tugba Erpek received the B.S. degree in Electrical Engineering from Osmangazi University, Eskisehir, Turkey, in 2005. She was a research assistant at Network Architecture and Performance Laboratory (NAPL) at George Mason University from 2005 to 2007. She is currently working at Shared Spectrum Company as a Systems Engineer. Her research interests include wireless communications and digital signal processing.